


SPACE–TIME REDUCED BASIS METHODS FOR PARAMETRIZED UNSTEADY STOKES EQUATIONS

 **Riccardo Tenderini**

Institute of Mathematics
École Polytechnique Fédérale de Lausanne (EPFL)
CH–1015 Lausanne, Switzerland

Nicholas Mueller

Department of Mathematics
Monash University
VIC–3800, Clayton, Victoria, Australia

 **Simone Deparis**

Institute of Mathematics
École Polytechnique Fédérale de Lausanne (EPFL)
CH–1015 Lausanne, Switzerland

ABSTRACT

In this work, we analyse space–time reduced basis methods for the efficient numerical simulation of hæmodynamics in arteries. The classical formulation of the reduced basis (RB) method features dimensionality reduction in space, while finite differences schemes are employed for the time integration of the resulting ordinary differential equation (ODE). Space–time reduced basis (ST–RB) methods extend the dimensionality reduction paradigm to the temporal dimension, projecting the full–order problem onto a low–dimensional spatio–temporal subspace. Our goal is to investigate the application of ST–RB methods to the unsteady incompressible Stokes equations, with a particular focus on stability. High-fidelity simulations are performed using the Finite Element (FE) method and BDF2 as time marching scheme. We consider two different ST–RB methods. In the first one — called ST–GRB — space–time model order reduction is achieved by means of a Galerkin projection; a spatio–temporal supremizers enrichment procedure is introduced to guarantee stability. The second method — called ST–PGRB — is characterized by a Petrov–Galerkin projection, stemming from a suitable minimization of the FOM residual, that allows to automatically attain stability. The classical RB method — denoted as SRB–TFO — serves as a baseline for the theoretical development. Numerical tests have been conducted on an idealized symmetric bifurcation geometry and on the patient–specific one of a femoropopliteal bypass. The results show that both ST–RB methods provide accurate approximations of the high–fidelity solutions, while considerably reducing the computational cost. In particular, the ST–PGRB method exhibits the best performance, as it features a better computational efficiency while retaining accuracies in accordance with theoretical expectations.

Keywords Hæmodynamics · Twofold saddle point problems · Reduced basis method · Space–time model order reduction · Supremizers enrichment · Least–squares Petrov–Galerkin projection

1 Introduction

Patient–specific high–fidelity numerical simulations of hæmodynamics are traditionally performed solving parametrized unsteady incompressible Navier–Stokes equations. The Finite Elements (FE) or the Finite Volumes (FV) methods are typically used for spatial discretization, while implicit linear multistep (as Backward Differentiation Formulas – BDF) or multistage (as Runge–Kutta – RK) methods are employed for the time integration of the resulting ordinary differential equation (ODE). Overall, this defines the so–called full–order model (FOM). Depending on the features of the problem at hand — like the shape and dimension of the physical domain, the complexity of the physical processes of interest or the length of the simulation interval — solving the FOM problem can be extremely expensive from a computational standpoint, even exploiting parallel computations [1]. In case of parametric dependence, Reduced Order Models (ROMs) are widely employed to lighten the computational burden of the simulations, yet retaining a good

degree of accuracy. Projection-based ROMs (PROMs) — as the traditional Reduced Basis (RB) method — reduce the spatial dimensionality of the dynamical system by means of a projection process, leading to a low-dimensional ODE. However, the resolution of the latter involves time integration, which is typically performed adopting the same scheme and with the same timestep size used in the FOM. As a result, traditional space-reduced ROMs feature a much smaller dimensionality in space than the FOM, but the same one in time. Therefore, in problems where either the time simulation interval is very large (as for instance in many applications in computational fluid dynamics), or the timestep size should be very small in order to capture some relevant behaviours happening at small time scales (as for instance in molecular dynamics), significant computational gains are difficult to realize.

The issue linked to temporal complexity has already been addressed in various ways. We refer the reader to [2] for a comprehensive literature review on the topic. A first idea is to employ a larger timestep size for the time integration of the low-dimensional ODE arising from the ROM, compared to the one employed for the FOM [3, 4, 5]. For suitable choices of the timestep size, stability issues can be circumvented. However, this approach may become problematic — in terms of accuracy — if the problem at hand features stiff dynamics. Time-parallel methods (as parareal [6], PITA [7] and MGRIT [8]) allow to parallelize numerical simulations in the temporal domain. However, only the wall-time of the simulations is reduced, while the temporal dimensionality of the problem is unchanged. “Forecasting” approaches allow to generate forecasts of the solution, which can then be used either as initial guesses for the Newton method [9] or to accelerate the convergence of time-parallel methods [10]. However, also these approaches only affect the wall-time of the simulations. Space-time ROMs — in the RB framework — allow to reduce both the spatial and the temporal dimensionality of the FOM, by means of a projection process onto a low-dimensional spatio-temporal basis [11, 12, 13, 14]. Additionally, they feature error bounds that grow linearly, rather than exponentially, with respect to the number of timesteps. However, these methods feature some relevant drawbacks, as the need for a (uncommon) FE discretization of the time domain and the absence of hyper-reduction techniques to efficiently handle non-linearities.

Reference [2] proposes a novel approach — called Space-Time Least-Squares Petrov-Galerkin (ST-LSPG) method — to tackle parametrized non-linear dynamical systems. The idea is to minimize the FOM residual, computed from the FOM reconstruction of the space-time reduced solution, in a weighted spatio-temporal ℓ^2 -norm. Different choices for the reduced basis construction and for the weighting matrix assembling are proposed and analysed. *A priori* error bounds, bounding the solution error by the best space-time approximation error, are also retrieved and the stability constant features a subquadratic growth with respect to the total number of time instances. Even though the performances of the ST-LSPG method are found to be good on 1D non-linear dynamical systems, a deterioration is expected when dealing with 2D or 3D geometries. This claim is particularly strong if the space-time collocation approach is employed for hyper-reduction, since sampling techniques notoriously suffer the curse of dimensionality. In [15], the drawbacks of the ST-LSPG method are addressed adopting a time-windowed strategy (Windowed ST-LSPG – WST-LSPG). The time simulation is partitioned into windows; within each window a low-dimensional spatio-temporal subspace is defined and the residual is minimized in a weighted ℓ^2 -norm. Numerical experiments, carried out also considering 2D compressible Navier-Stokes equations for the flow around an airfoil, demonstrate that the WST-LSPG method is better than the ST-LSPG one both in terms of accuracy and of efficiency. However, the coupling between the different time windows is not taken into account and this could easily deteriorate the performances if their number is large. Finally, in [16, 17], the time-complexity bottleneck of the RB method is addressed by performing, respectively, a Galerkin projection and a least-squares Petrov-Galerkin projection of the FOM onto a low-dimensional spatio-temporal subspace. The resulting methods exhibit good performances on 2D linear dynamical systems and *a priori* error bounds featuring a subquadratic dependency on the total number of time instants are derived. However, only linear problems have been considered.

The goal of this work is to investigate the application of Space-Time Reduced Basis (ST-RB) methods to the unsteady parametrized incompressible Stokes equations, a well-known linearization of the Navier-Stokes equations that models Newtonian flow at small Reynolds’ numbers ($Re \ll 1$). The parametrization of the problem affects the inflow and the outflow rates, while the geometry is assumed fixed. Additionally, non-homogeneous Dirichlet boundary conditions (BCs) are weakly imposed by means of Lagrange multipliers [18]. The application of two different ST-RB methods — which rely on a Galerkin and on a Petrov-Galerkin projection respectively — to the problem at hand is detailed and their stability is analysed. This last step is particularly important, as we deal with a twofold saddle point problem [19, 20].

The manuscript is structured as follows. In Section 2, we introduce the unsteady parametrized incompressible Stokes equations and we discuss their full-order discretization. In Section 3, we investigate the application of the aforementioned ST-RB approaches to the problem at hand. In particular, we detail the construction of the space-time reduced bases and, for both methods, we detail the assembling of the linear systems to be solved. Additionally, we discuss the stability of the two approaches. Section 4 presents the numerical results, obtained on two different test cases, characterized by different geometries and parametrizations of the boundary data. Finally, Section 5 provides a final summary, lists the main limitations of the work and proposes some possible further developments.

2 Unsteady Parametrized Incompressible Stokes Equations

Even if hæmorheology indicates that blood is a non-Newtonian fluid, the latter can be approximated as a Newtonian one if the vessels where it flows are sufficiently large. Under this assumption, the blood flow is governed by unsteady incompressible Navier–Stokes equations. In this work, we make an additional simplification: we neglect the non-linear convective term characterizing the Navier–Stokes equations, thus modelling blood flow by means of the unsteady incompressible Stokes equations. This system of linear PDEs well describes incompressible Newtonian flow at small Reynolds’ numbers ($Re \ll 1$), i.e. in a regime where advective inertial forces are negligible with respect to viscous ones (see e.g. [21, 22]).

2.1 Strong and weak formulation

We consider an open, simply connected and bounded domain $\Omega \subset \mathbb{R}^d$ and we denote its boundary by $\partial\Omega$. The unsteady parametrized incompressible Stokes equations in Ω read as:

$$\begin{cases} \rho \underline{u}_t^\mu - \nabla \cdot (2\mu \nabla^s \underline{u}^\mu) + \nabla p^\mu = \underline{f}^\mu & \text{in } \Omega \times [0, T] \\ \nabla \cdot \underline{u}^\mu = 0 & \text{in } \Omega \times [0, T] \\ \underline{u}^\mu = \underline{g}^\mu & \text{on } \Gamma_D \times [0, T] \\ \sigma(\underline{u}^\mu, p^\mu) \underline{n} = \underline{h}^\mu & \text{on } \Gamma_N \times [0, T] \\ \underline{u}^\mu = \underline{u}_0^\mu & \text{in } \Omega \times \{0\} \end{cases} \quad (2.1)$$

where $\underline{u}^\mu : \Omega \times [0, T] \rightarrow \mathbb{R}^d$ and $p^\mu : \Omega \times [0, T] \rightarrow \mathbb{R}$ are the velocity and the pressure of the fluid (\underline{u}_t^μ denotes the partial derivative of the velocity in time); ρ and μ are the fluid’s density and viscosity respectively; $\nabla^s \underline{u} = (\nabla \underline{u} + \nabla^T \underline{u})/2$ is the strain rate tensor; $\sigma(\underline{u}, p) = 2\mu \nabla^s \underline{u} - pI$ is the Cauchy stress tensor; $\underline{f}^\mu : \Omega \times [0, T] \rightarrow \mathbb{R}^d$ is a forcing term; $\underline{g}^\mu : \Gamma_D \times [0, T] \rightarrow \mathbb{R}^d$ and $\underline{h}^\mu : \Gamma_N \times [0, T] \rightarrow \mathbb{R}^d$ are the Dirichlet and Neumann boundary data, respectively; $\underline{u}_0^\mu : \Omega \rightarrow \mathbb{R}^d$ is the initial condition; \underline{n} is the outward unit normal vector to $\partial\Omega$. $\{\Gamma_D, \Gamma_N\}$ is a partition of $\partial\Omega$ which defines the Dirichlet and the Neumann boundaries, respectively. As we deal with cardiovascular simulations, it is useful to define the inlet boundary Γ_{IN} , the outlet boundary Γ_{OUT} and the vessel wall boundary Γ_W . In this work, we always impose homogeneous Dirichlet BCs on Γ_W (i.e. no-slip BCs, so that the artery is approximated as a rigid object) and non-homogeneous Dirichlet BCs on Γ_{IN} . The nature of the BCs imposed on Γ_{OUT} depends instead on the test case at hand. We also define the non-homogeneous Dirichlet boundary $\tilde{\Gamma}_D := \bigcup_{k=1}^{N_D} \tilde{\Gamma}_D^k$, where $\tilde{\Gamma}_D^k$ denotes the k -th inlet/outlet boundary where non-homogeneous Dirichlet BCs are imposed; N_D is the number of such boundaries. $\mathcal{D} \subset \mathbb{R}^p$ defines the parameter space and we generically denote by μ one of its elements. In particular, here we consider the dependence on μ to exclusively characterize the Dirichlet datum \underline{g}^μ . This restriction allows for an efficient offline/online splitting; other choices are of course possible. For the sake of conciseness, from now on we drop all the $(\cdot)^\mu$ superscripts, except when referring to the Dirichlet datum \underline{g}^μ .

Let us introduce the following spaces:

$$\mathcal{V}^g := (H^1|_{\Gamma_D}(\Omega))^d = \{ \underline{v} \in (H^1(\Omega))^d \text{ s.t. } \underline{v} = \underline{g}^\mu \text{ on } \Gamma_D \}; \quad \mathcal{Q} := L^2(\Omega); \quad (2.2)$$

equipped with the usual inner products $(\cdot, \cdot)_{\mathcal{V}^g} = (\cdot, \cdot)_{(H^1)^d}$ and $(\cdot, \cdot)_{\mathcal{Q}} = (\cdot, \cdot)_{L^2}$. Let us also define $\mathcal{V}_0 := (H_0^1(\Omega))^d$. The weak formulation of Eq.(2.1) has the structure of a non-symmetric and non-coercive saddle point problem. Instead of relying on the definition of a lifting function, we choose to impose non-homogeneous Dirichlet BCs weakly, using Lagrange multipliers. Such a choice is driven by the possibility of using a similar formulation to couple several domains [18]. This approach translates into the following weak formulation:

Problem 1. Given \underline{f} , \underline{g}^μ , \underline{h} regular enough, find $(\underline{u}, p, \underline{\lambda}) \in \mathcal{V}^g \times \mathcal{Q} \times \mathcal{L}$, such that $\forall t \in [0, T]$:

$$\begin{cases} \rho \int_\Omega \underline{u}_t \cdot \underline{v} + \mu \int_\Omega \nabla^s \underline{u} : \nabla^s \underline{v} - \int_\Omega p \nabla \cdot \underline{v} + \int_{\tilde{\Gamma}_D} \underline{\lambda} \cdot \underline{v} = \int_\Omega \underline{f} \cdot \underline{v} + \int_{\Gamma_N} \underline{h} \cdot \underline{v} & \forall \underline{v} \in \mathcal{V}^0 \\ \int_\Omega q \nabla \cdot \underline{u} = 0 & \forall q \in \mathcal{Q} \\ \int_{\tilde{\Gamma}_D} \underline{u} \cdot \underline{\xi} = \int_{\tilde{\Gamma}_D} \underline{g}^\mu \cdot \underline{\xi} & \forall \underline{\xi} \in \mathcal{L} \end{cases} \quad (2.3)$$

and $\underline{u} = \underline{u}_0$ for $t = 0$.

Based on the theory on primal hybrid methods (see e.g. [18]), a natural choice for the space of Lagrange multipliers is

$\mathcal{L} := \prod_{k=1}^{N_D} \mathcal{L}^k$, with $\mathcal{L}^k = \left(H_{00}^{-1/2}(\tilde{\Gamma}_D^k) \right)^d$ being the dual space of

$$\left(H_{00}^{1/2}(\tilde{\Gamma}_D^k) \right)^d := \left\{ \underline{\eta} \in \left(H^{1/2}(\tilde{\Gamma}_D^k) \right)^d : E^0 \underline{\eta} \in \left(H^{1/2}(\partial\Omega) \right)^d \right\} \quad (2.4)$$

Here $E^0\eta$ is the trivial extension by 0 of η to $\partial\Omega$. We remark that Problem 1 features a twofold saddle point structure, as the dual space $\mathcal{Q} \times \mathcal{L}$ is a product space [19, 20].

2.2 Numerical Discretization

As Problem 1 is time-dependent, its discretization involves both the spatial and the temporal dimension. Concerning spatial discretization, we rely on the FE method. Therefore, we introduce the following finite dimensional approximations of velocity, pressure and Lagrange multipliers (for $k \in \{1, \dots, N_D\}$):

$$\underline{u}_h(\mathbf{x}, t) = \sum_{i=1}^{N_u^s} u_i(t) \underline{\varphi}_i^u(\mathbf{x}) \in \mathcal{V}_h^g, \quad p_h(\mathbf{x}, t) = \sum_{i=1}^{N_p^s} p_i(t) \varphi_i^p(\mathbf{x}) \in \mathcal{Q}_h, \quad \underline{\lambda}_h^k = \sum_{i=1}^{N_\lambda^k} \lambda_i^k(t) \underline{\eta}_i^k(\mathbf{x}) \in \mathcal{L}_h^k. \quad (2.5)$$

The definitions of \mathcal{V}_h^g and \mathcal{Q}_h are of key importance for the accuracy of the approximation. Moreover, in the case of saddle point problems, the quality of the discretization is critical to ensure well-posedness; we refer to Section 2.3 for details. The discretization of the spaces of Lagrange multipliers is based on the definition of orthonormal basis functions on the unit disk \mathcal{D} which are constructed from Chebyshev polynomials of the second kind. Since $\mathcal{L} := \prod_{k=1}^{N_D} \mathcal{L}^k$, we have that $\mathcal{L}_h = \prod_{k=1}^{N_D} \mathcal{L}_h^k$, where \mathcal{L}_h^k is a finite-dimensional approximation of \mathcal{L}^k . This implies that the dimensionality of \mathcal{L}_h is $N_\lambda = \sum_{k=1}^{N_D} N_\lambda^k$, being $N_\lambda^k := \dim(\mathcal{L}_h^k)$. We denote the basis functions of \mathcal{L}_h^k as $\{\underline{\eta}_i^k\}_{i=1}^{N_\lambda^k}$; they are orthonormal in $L^2(\tilde{\Gamma}_D^k)$ -norm. We refer the reader to [18] for additional details. Let us introduce the following matrices and vectors

$$\begin{aligned} \mathbf{A} \in \mathbb{R}^{N_u^s \times N_u^s} : \quad \mathbf{A}_{ij} &= 2\mu \int_{\Omega} \nabla^s(\underline{\varphi}_j^u) : \nabla^s(\underline{\varphi}_i^u) & \mathbf{M} \in \mathbb{R}^{N_u^s \times N_u^s} : \quad \mathbf{M}_{ij} &= \rho \int_{\Omega} \underline{\varphi}_j^u \cdot \underline{\varphi}_i^u \\ \mathbf{B} \in \mathbb{R}^{N_p^s \times N_u^s} : \quad \mathbf{B}_{ij} &= - \int_{\Omega} \varphi_i^p \nabla \cdot \underline{\varphi}_j^u & \mathbf{C}^k \in \mathbb{R}^{N_\lambda^k \times N_u^s} : \quad \mathbf{C}_{ij}^k &= \int_{\tilde{\Gamma}_D^k} \underline{\varphi}_j^u \cdot \underline{\eta}_i^k \\ \mathbf{f} \in \mathbb{R}^{N_u^s} : \quad \mathbf{f}_i &= \int_{\Omega} \underline{f} \cdot \underline{\varphi}_i^u + \int_{\Gamma_N} \underline{h} \cdot \underline{\varphi}_i^u & \tilde{\mathbf{g}}^{k,\mu} \in \mathbb{R}^{N_\lambda^k} : \quad \tilde{\mathbf{g}}_i^{k,\mu} &= \int_{\tilde{\Gamma}_D^k} \underline{g}^{k,\mu} \cdot \underline{\eta}_i^k \end{aligned} \quad (2.6)$$

where $\underline{g}^{k,\mu}$ represents the Dirichlet datum on $\tilde{\Gamma}_D^k$. To ease the notation, we also define

$$\mathbf{C} = [(\mathbf{C}^1)^T \mid \dots \mid (\mathbf{C}^{N_D})^T]^T \in \mathbb{R}^{N_\lambda \times N_u^s}, \quad \tilde{\mathbf{g}}^\mu = [(\tilde{\mathbf{g}}^{1,\mu})^T \mid \dots \mid (\tilde{\mathbf{g}}^{N_D,\mu})^T]^T \in \mathbb{R}^{N_\lambda}. \quad (2.7)$$

The semi-discretization in space of Problem 1 can be then written in the form of a multi-dimensional Ordinary Differential Equation (ODE) as follows:

$$\begin{bmatrix} \mathbf{M} \\ \mathbf{A} \\ \mathbf{B}^T \\ \mathbf{C}^T \end{bmatrix} \begin{bmatrix} \mathbf{u}_t \\ \mathbf{p}_t \\ \underline{\lambda}_t \end{bmatrix} + \begin{bmatrix} \mathbf{A} & \mathbf{B}^T & \mathbf{C}^T \\ \mathbf{B} & \mathbf{C} & \mathbf{0} \end{bmatrix} \begin{bmatrix} \mathbf{u} \\ \mathbf{p} \\ \underline{\lambda} \end{bmatrix} = \begin{bmatrix} \mathbf{f}(t) \\ \mathbf{0} \\ \tilde{\mathbf{g}}^\mu(t) \end{bmatrix} \quad (2.8)$$

where $\mathbf{u}(t) \in \mathbb{R}^{N_u^s}$, $\mathbf{p}(t) \in \mathbb{R}^{N_p^s}$ and $\underline{\lambda}(t) = [\underline{\lambda}_1^T, \dots, \underline{\lambda}_{N_D}^T]^T \in \mathbb{R}^{N_\lambda}$ are the vectors of degrees of freedom (DOFs) at time $t \in [0, T]$. Blocks of zeros are left empty to simplify the notation.

Remark. Notice that, in order to strongly enforce homogeneous Dirichlet BCs on the vessel wall Γ_W , we need to suitably modify the rows of the matrices \mathbf{M} , \mathbf{A} , \mathbf{B}^T , \mathbf{C}^T and \mathbf{f} . As a result, \mathbf{B}^T and \mathbf{C}^T do not exactly correspond to the transposed of \mathbf{B} and \mathbf{C} , respectively.

Regarding temporal discretization, let us introduce a sequence of timesteps $\{t_n\}_{n=0}^{N^t}$ such that $t_0 = 0$, $t_{N^t} = T$ and $t_{n+1} = t_n + \delta$; $\delta = T/N^t$ is called timestep size. Let $\mathbf{w}_k := [\mathbf{u}_k, \mathbf{p}_k, \underline{\lambda}_k]^T \in \mathbb{R}^{N^s}$ is the solution at time t_k , with $N^s := N_u^s + N_p^s + N_\lambda$ and for $k \in \{0, \dots, N^t\}$. We apply the second-order implicit BDF2 scheme. So, given \mathbf{w}_{n-j+1} for $j = 1, 2$, the numerical solution at time t_{n+1} is such that:

$$\mathbf{r}(\mathbf{w}_{n+1}) := \mathbf{H} \mathbf{w}_{n+1} - \sum_{j=1}^2 \alpha_j \mathbf{H} \mathbf{w}_{n-j+1} - \delta \beta \tilde{\mathbf{f}}(t_{n+1}, \mathbf{w}_{n+1}) = \mathbf{0} \quad (2.9)$$

where

$$\mathbf{H} = \begin{bmatrix} \mathbf{M} \\ \mathbf{A} \\ \mathbf{B}^T \\ \mathbf{C}^T \end{bmatrix} \quad \tilde{\mathbf{f}}(t_n, \mathbf{w}_n) = \begin{bmatrix} \mathbf{f}(t_n) \\ \mathbf{0} \\ \tilde{\mathbf{g}}^\mu(t_n) \end{bmatrix} - \begin{bmatrix} \mathbf{A} & \mathbf{B}^T & \mathbf{C}^T \\ \mathbf{B} & \mathbf{C} & \mathbf{0} \end{bmatrix} \begin{bmatrix} \mathbf{u}_n \\ \mathbf{p}_n \\ \underline{\lambda}_n \end{bmatrix} \quad (2.10)$$

In particular, for the BDF2 method, we have $\alpha_1 = 4/3$, $\alpha_2 = -1/3$ and $\beta = 2/3$.

Eq.(2.9) can be rewritten in the form of a single linear system of dimension $N^{st} \times N^{st}$ — being $N^{st} := N^s N^t$ the number of DOFs of the space–time FOM problem — as:

$$\begin{bmatrix} \mathbf{A}_1^{st} & \mathbf{A}_2^{st} & \mathbf{A}_3^{st} \\ \mathbf{A}_4^{st} & & \\ \mathbf{A}_7^{st} & & \end{bmatrix} \begin{bmatrix} \mathbf{u}^{st} \\ \mathbf{p}^{st} \\ \boldsymbol{\lambda}^{st} \end{bmatrix} = \begin{bmatrix} \mathbf{F}_1^{st} \\ \mathbf{F}_3^{st}(\boldsymbol{\mu}) \end{bmatrix} \quad (2.11)$$

or, even more compactly, as $\mathbf{A}^{st} \mathbf{w}^{st} = \mathbf{F}_\mu^{st}$. The blocks of matrix \mathbf{A}^{st} , that features a twofold saddle point structure of type 1 [20], can be written as follows:

$$\begin{aligned} \mathbf{A}_1^{st} &= \text{diag}\left(\underbrace{\mathbf{M}, \dots, \mathbf{M}}_{N^t}\right) + \frac{2}{3}\delta \text{diag}\left(\underbrace{\mathbf{A}, \dots, \mathbf{A}}_{N^t}\right) \\ &\quad - \frac{4}{3} \text{subdiag}^{(1)}\left(\underbrace{\mathbf{M}, \dots, \mathbf{M}}_{N^t-1}\right) + \frac{1}{3} \text{subdiag}^{(2)}\left(\underbrace{\mathbf{M}, \dots, \mathbf{M}}_{N^t-2}\right) \\ \mathbf{A}_2^{st} &= \frac{2}{3}\delta \text{diag}\left(\underbrace{\mathbf{B}^T, \dots, \mathbf{B}^T}_{N^t}\right) & \mathbf{A}_3^{st} &= \frac{2}{3}\delta \text{diag}\left(\underbrace{\mathbf{C}^T, \dots, \mathbf{C}^T}_{N^t}\right) \\ \mathbf{A}_4^{st} &= \text{diag}\left(\underbrace{\mathbf{B}, \dots, \mathbf{B}}_{N^t}\right) & \mathbf{A}_7^{st} &= \text{diag}\left(\underbrace{\mathbf{C}, \dots, \mathbf{C}}_{N^t}\right) \end{aligned} \quad (2.12)$$

Here $\text{diag} : \mathbb{R}^{r_1 \times c_1} \times \dots \times \mathbb{R}^{r_K \times c_K} \rightarrow \mathbb{R}^{(r_1 + \dots + r_K) \times (c_1 + \dots + c_K)}$ is the function that builds a block diagonal matrix from a set of K input matrices; $\text{subdiag}^{(n)}$ ($n \in \mathbb{N}$) is equivalent to diag , but with respect to the n -th lower-diagonal. Before reporting the expressions of the blocks appearing in the right-hand side vector of Eq.(2.11), let us make some additional assumptions:

1. We assume that $\mathbf{f}(t) = \mathbf{0} \forall t \in [0, T]$. This implies, for instance, that we neglect the effect of gravity. We also assume that $\mathbf{h}(t) = \mathbf{0} \forall t \in [0, T]$, which means that we only deal with homogeneous Neumann BCs.
2. We assume that $\mathbf{u}_0 = \mathbf{0}$ in Ω . Moreover, we suppose that $\mathbf{u}(t) = \mathbf{0} \forall t \leq 0$, so that the BDF2 scheme can also be safely employed in the first iteration.
3. For all $k \in \{1, \dots, N_D\}$, we assume that the Dirichlet datum $\underline{g}^{k, \mu}$ on $\tilde{\Gamma}_D^k$ can be factorized as:

$$\underline{g}^{k, \mu}(\mathbf{x}, t) = \underline{g}_k^s(\mathbf{x}) g_k^t(t; \boldsymbol{\mu}) \quad \text{for } (\mathbf{x}, t) \in \tilde{\Gamma}_D^k \times [0, T] \quad (2.13)$$

Thus, we have that $\tilde{\mathbf{g}}^{k, \mu}(t) = \tilde{\mathbf{g}}_k^s g_k^t(t; \boldsymbol{\mu})$, where $\tilde{\mathbf{g}}_k^s \in \mathbb{R}^{N_\lambda^k}$ is such that $(\tilde{\mathbf{g}}_k)_i = \int_{\tilde{\Gamma}_D^k} \underline{g}_k^s \cdot \boldsymbol{\eta}_i^k$.

Assumptions 1 and 2 imply that $\mathbf{F}_1^{st} = \mathbf{0}$. Therefore, the only non-zero block in \mathbf{F}_μ^{st} is $\mathbf{F}_3^{st} \in \mathbb{R}^{N_\lambda N^t}$ and it writes as

$$\mathbf{F}_3^{st}(\boldsymbol{\mu}) = \begin{bmatrix} \tilde{\mathbf{g}}^{st}(t_1; \boldsymbol{\mu}) \\ \vdots \\ \tilde{\mathbf{g}}^{st}(t_{N^t}; \boldsymbol{\mu}) \end{bmatrix} \quad \text{with} \quad \tilde{\mathbf{g}}^{st}(t_k; \boldsymbol{\mu}) = \begin{bmatrix} \tilde{\mathbf{g}}_1^s g_1^t(t_k; \boldsymbol{\mu}) \\ \vdots \\ \tilde{\mathbf{g}}_{N_D}^s g_{N_D}^t(t_k; \boldsymbol{\mu}) \end{bmatrix}. \quad (2.14)$$

2.3 Well-posedness of the FOM problem

As we pointed out in Subsections 2.1–2.2, Problem 1 features a twofold saddle point structure of type 1. In particular, the velocity is the primal variable, whereas pressure and Lagrange multipliers — associated to the weak imposition of inhomogeneous Dirichlet BCs — are the dual ones. As discussed in [19, 20], necessary and sufficient conditions for its well-posedness can be expressed by means of suitable *inf-sup* conditions, which need to be satisfied both at continuous and at discrete level. As in [18], we assume Problem 1 to be well-posed in the continuous setting and we directly focus on the conditions to be enforced at discrete level. Based on classical theoretical results on the well-posedness of saddle point problems (see e.g. [23, 24, 25]), adopting an algebraic standpoint, the following inequality must hold

$$\exists \beta_F > 0 : \inf_{(q, \boldsymbol{\lambda}) \neq \mathbf{0}} \sup_{\mathbf{v} \neq \mathbf{0}} \frac{\mathbf{q}^T \mathbf{B} \mathbf{v} + \boldsymbol{\lambda}^T \mathbf{C} \mathbf{v}}{\|\mathbf{v}\|_{\mathbf{x}_u} (\|\mathbf{q}\|_{\mathbf{x}_p} + \|\boldsymbol{\lambda}\|_{\mathbf{x}_\lambda})} \geq \beta_F \quad (2.15)$$

\mathbf{X}_u , \mathbf{X}_p and \mathbf{X}_λ are symmetric and positive-definite matrices, defined as follows:

$$\mathbf{X}_u = \frac{1}{\rho} \mathbf{M} + \frac{1}{2\mu} \mathbf{A} \in \mathbb{R}^{N_u^s \times N_u^s} \quad \mathbf{X}_p = \mathbf{M}^p \in \mathbb{R}^{N_p^s \times N_p^s} \quad \mathbf{X}_\lambda = \mathbf{I}_{N_\lambda} \in \mathbb{R}^{N_\lambda \times N_\lambda} \quad (2.16)$$

Theorem 3.1 in [20] states that Eq.(2.15) can be equivalently expressed in the two following ways:

$$\exists \beta_F > 0 : \inf_{\mathbf{q} \neq \mathbf{0}} \sup_{\mathbf{v} \neq \mathbf{0}} \frac{\mathbf{q}^T \mathbf{B} \mathbf{v}}{\|\mathbf{v}\|_{\mathbf{X}_u} \|\mathbf{q}\|_{\mathbf{X}_p}} \geq \beta_F \quad \text{and} \quad \inf_{\lambda \neq 0} \sup_{\substack{\mathbf{v} \neq \mathbf{0} \\ \mathbf{B} \mathbf{v} = \mathbf{0}}} \frac{\lambda^T \mathbf{C} \mathbf{v}}{\|\mathbf{v}\|_{\mathbf{X}_u} \|\lambda\|_{\mathbf{X}_\lambda}} \geq \beta_F \quad (2.17a)$$

$$\exists \beta_F > 0 : \inf_{\mathbf{q} \neq \mathbf{0}} \sup_{\substack{\mathbf{v} \neq \mathbf{0} \\ \mathbf{C} \mathbf{v} = \mathbf{0}}} \frac{\mathbf{q}^T \mathbf{B} \mathbf{v}}{\|\mathbf{v}\|_{\mathbf{X}_u} \|\mathbf{q}\|_{\mathbf{X}_p}} \geq \beta_F \quad \text{and} \quad \inf_{\lambda \neq 0} \sup_{\mathbf{v} \neq \mathbf{0}} \frac{\lambda^T \mathbf{C} \mathbf{v}}{\|\mathbf{v}\|_{\mathbf{X}_u} \|\lambda\|_{\mathbf{X}_\lambda}} \geq \beta_F \quad (2.17b)$$

Therefore, on the one side the *inf-sup* stability of Problem 1 in the discrete setting is guaranteed if two distinct *inf-sup* inequalities — one for each of the dual fields — are satisfied. However, on the other side, one of the two *inf-sup* inequalities features an additional constraint on the primal variable. Thus, the independent fulfilment of the conventional *inf-sup* conditions on the dual variables is not enough to guarantee well-posedness.

In this work, we claim the well-posedness of Problem 1 in the discrete framework by considering Eq.(2.17a), where the first inequality (related to pressure) is “standard”, while the second one (related to Lagrange multipliers) features a supremum taken over velocities that satisfy the constraint $\mathbf{B} \mathbf{v} = \mathbf{0}$ (i.e. weakly divergence-free velocities). Proceeding as in [18], on the one hand we guarantee the fulfilment of the first inequality in Eq.(2.17a) by employing $P2 - P1$ Taylor-Hood Lagrangian finite elements [26] (i.e. piecewise polynomials of order 2 for the velocity and of order 1 for the pressure, built on a tetrahedral triangulation of the domain Ω), which are the most popular example of stable discretization couple. On the other hand, instead, we only assess the second inequality empirically, by computing the condition number of the system matrix in Eq.(2.8). In all our numerical tests (see Section 5) the FOM system matrix proved to be well-conditioned, thus suggesting the well-posedness of the problem at hand.

3 Space-time reduced basis methods for parametrized unsteady incompressible Stokes equations

Classical applications of ROMs to parametrized PDEs (and to dynamical systems in general) allow to reduce only spatial dimensionality, since the projection process takes place with respect to the spatial subspaces where the solution is sought at every time instant. Conversely, the temporal dimensionality of the problem does not change upon the reduction step, as the ODE stemming from the semi-discrete ROM is solved by means of numerical integration, typically with the same time integrator and timestep size employed for the FOM. Because of this, classical ROMs are characterized by a low dimensionality in space, but by a high one in time, which may limit the computational savings. This aspect could be particularly relevant in problems where either the simulation interval should be very large, as in many applications in computational fluid dynamics, or the timestep size should be very small, like in molecular dynamics simulations, in order to properly capture some relevant behaviours. As discussed in Section 1, several attempts to solve this temporal-complexity bottleneck have been made. Among those, in this work we focus on Space-Time Reduced Basis (ST-RB) methods, firstly introduced in [11, 12, 13, 14] and further developed in [2, 16, 17].

3.1 ST-RB problem definition

ST-RB methods allow to get dimensionality reduction also in time by projecting the FOM problem onto a low-dimensional spatio-temporal subspace, spanned by a suitable set of basis functions. We denote the spatio-temporal basis functions by $\pi_i^u \in \mathbb{R}^{N_u^s N^t}$ ($i \in \{1, \dots, n_u^{st}\}$) for the velocity, $\pi_i^p \in \mathbb{R}^{N_p^s N^t}$ ($i \in \{1, \dots, n_p^{st}\}$) for the pressure and $\pi_i^\lambda \in \mathbb{R}^{N_\lambda^s N^t}$ ($i \in \{1, \dots, n_\lambda^{st}\}$) for the Lagrange multipliers. The basis functions are generated by applying a truncated POD algorithm to the snapshots' tensor, storing the FOM solutions got during the so-called offline phase of the method for N_μ randomly selected parameter values $\{\mu_i\}_{i=1}^{N_\mu}$, with $\mu_i \in \mathcal{D}$. By construction the basis functions are orthonormal with respect to a suitable norm; a more detailed explanation is given in Subsection 3.2. In this framework, the discrete manifold of FOM solutions is approximated by the following low-dimensional subspace

$$\begin{aligned} \mathcal{ST}_{h,\delta}^u &= \text{span}\{\pi_i^u\}_{i=1}^{n_u^{st}} \\ \mathcal{ST}_{h,\delta} &= \mathcal{ST}_{h,\delta}^u \times \mathcal{ST}_{h,\delta}^p \times \mathcal{ST}_{h,\delta}^\lambda \quad \text{with} \quad \mathcal{ST}_{h,\delta}^p = \text{span}\{\pi_i^p\}_{i=1}^{n_p^{st}} \\ \mathcal{ST}_{h,\delta}^\lambda &= \text{span}\{\pi_i^\lambda\}_{i=1}^{n_\lambda^{st}} \end{aligned} \quad (3.1)$$

Additionally, we define $n^{st} := n_u^{st} + n_p^{st} + n_\lambda^{st}$ as the dimension of $\mathcal{ST}_{h,\delta}$. The basis of $\mathcal{ST}_{h,\delta}$ can be encoded in the matrix $\mathbf{\Pi}$, defined as follows:

$$\mathbf{\Pi} = \text{diag}\left(\left[\pi_1^u | \dots | \pi_{n_u^{st}}^u\right], \left[\pi_1^p | \dots | \pi_{n_p^{st}}^p\right], \left[\pi_1^\lambda | \dots | \pi_{n_\lambda^{st}}^\lambda\right]\right) = \text{diag}\left(\mathbf{\Pi}^u, \mathbf{\Pi}^p, \mathbf{\Pi}^\lambda\right) \in \mathbb{R}^{N^{st} \times n^{st}}. \quad (3.2)$$

The function $diag$ is defined as in Eq.(2.12). We remark that, thanks to the orthonormality of the basis functions, the matrix $\mathbf{\Pi}$ identifies a projection operator (in a suitable norm), going from the spatio-temporal FOM space of dimension N^{st} to the spatio-temporal reduced subspace $\mathcal{ST}_{h,\delta}$, of dimension $n^{st} \ll N^{st}$.

Adopting an algebraic perspective and employing the compact notation introduced in Eq.(2.11), the application of ST-RB methods amounts at solving the following problem:

$$\text{Find } \hat{\mathbf{w}} \in \mathbb{R}^{n^{st}} \text{ such that } \tilde{\mathbf{\Pi}}^T (\mathbf{F}_\mu^{st} - \mathbf{A}^{st} \mathbf{\Pi} \hat{\mathbf{w}}) = \mathbf{0}, \quad (3.3)$$

where $\tilde{\mathbf{\Pi}} \in \mathbb{R}^{N^{st} \times n^{st}}$ is a projection matrix, possibly equal to $\mathbf{\Pi}$. Based on the definition of $\mathbf{\Pi}$ given in Eq.(3.2), the term $\mathbf{\Pi} \hat{\mathbf{w}}$ represents a linear combination of the reduced basis elements, whose weights are given by the entries of $\hat{\mathbf{w}} \in \mathbb{R}^{n^{st}}$. Such term represents then the FOM reconstruction of the space-time reduced solution. So, the quantity $\mathbf{r}_\mu^{st} := \mathbf{F}_\mu^{st} - \mathbf{A}^{st} \mathbf{\Pi} \hat{\mathbf{w}}$ identifies the FOM residual associated to the space-time reduced solution. In Eq.(3.3) we are imposing such a residual to be orthogonal to some low-dimensional spatio-temporal subspace, whose basis is encoded in the projection matrix $\tilde{\mathbf{\Pi}}$. Notice that, if we focus on spatial discretization, this amounts at performing a (Petrov-)Galerkin projection as in the classical formulation of the RB method, featuring dimensionality reduction only along the spatial dimension [27]. In particular, a Galerkin projection is performed if $\tilde{\mathbf{\Pi}} = \mathbf{\Pi}$ and a Petrov-Galerkin projection otherwise. A similar interpretation could be given in terms of temporal discretization. However, the employment of a finite differences scheme for the time integration of the ODE in Eq.(2.8) prevents from identifying Eq.(3.3) with a (Petrov-)Galerkin projection. Ultimately, rearranging the terms in Eq.(3.3), the ST-RB problem writes as follows.

Problem 2. Find $\hat{\mathbf{w}} \in \mathbb{R}^{n^{st}}$ such that

$$\begin{aligned} \hat{\mathbf{A}}^{st} \hat{\mathbf{w}} &= \hat{\mathbf{F}}_\mu^{st} \quad \text{with} \quad \hat{\mathbf{A}}^{st} = \tilde{\mathbf{\Pi}}^T \mathbf{A}^{st} \mathbf{\Pi} \in \mathbb{R}^{n^{st} \times n^{st}} \\ \hat{\mathbf{F}}_\mu^{st} &= \tilde{\mathbf{\Pi}}^T \mathbf{F}_\mu^{st} \in \mathbb{R}^{n^{st}} \end{aligned} \quad (3.4)$$

3.2 Offline phase: reduced basis generation with POD

Let us consider a set of N_μ FOM velocity snapshots $\{\mathbf{u}_h^{st}(\mu_k)\}_{k=1}^{N_\mu}$, with $\mathbf{u}_h^{st}(\mu_k) \in \mathbb{R}^{N_u^s \times N^t}$, computed by solving Eq.(2.11) for N_μ different parameter values. These snapshots are stored in a third-order tensor $\chi^u \in \mathbb{R}^{N_u^s \times N^t \times N_\mu}$ so that

$$\chi_{ijk}^u = (\mathbf{u}_h^{st}(\mu_k))_{ij}, \quad i \in \{1, \dots, N_u^s\}, j \in \{1, \dots, N^t\}, k \in \{1, \dots, N_\mu\}. \quad (3.5)$$

Firstly, let us focus on the construction of the reduced basis in space, that at discrete level can be encoded in the matrix $\Phi^u \in \mathbb{R}^{N_u^s \times n_u^s}$. We want the reduced basis to be orthonormal with respect to the norm induced by the matrix \mathbf{X}_u (see Eq.(2.16)), which is indeed the $(H^1(\Omega))^d$ -norm. Denoting with $\mathbf{H}_u \in \mathbb{R}^{N_u^s \times N_u^s}$ the upper triangular matrix arising from the Cholesky decomposition of \mathbf{X}_u (i.e. $\mathbf{X}_u = \mathbf{H}_u^T \mathbf{H}_u$) and with $\chi_{(1)}^u \in \mathbb{R}^{N_u^s \times N^t N_\mu}$ the mode-1 unfolding of χ^u (see e.g. [2]), we perform the Singular Value Decomposition of $\mathbf{H}_u \chi_{(1)}^u$:

$$\mathbf{H}_u \chi_{(1)}^u = \mathbf{V} \mathbf{\Sigma} \mathbf{Z}^T. \quad (3.6)$$

$\mathbf{V} \in \mathbb{R}^{N_u^s \times N_u^s}$ and $\mathbf{Z} \in \mathbb{R}^{N^t N_\mu \times N^t N_\mu}$ are orthogonal matrices, whereas $\mathbf{\Sigma} \in \mathbb{R}^{N_u^s \times N^t N_\mu}$ is the pseudo-diagonal matrix storing the singular values $\{\sigma_i\}_{i=1}^{N_\sigma}$ of $\mathbf{H}_u \chi_{(1)}^u$ (with $N_\sigma := \min(N_u^s, N^t N_\mu)$ and $\sigma_i \geq 0 \forall i \in \{1, \dots, N_\sigma\}$). If the singular values are sorted in decreasing order and if we denote by $\tilde{\Phi}^u = [\phi_1^u | \dots | \phi_{n_u^s}^u] \in \mathbb{R}^{N_u^s \times n_u^s}$ the matrix formed by the first $n_u^s \ll N_u^s$ columns of \mathbf{V} , then the velocity reduced basis in space can be computed as $\Phi^u = \mathbf{H}_u^T \tilde{\Phi}^u$. The columns of the matrix Φ^u represent the n_u^s -dimensional orthonormal basis that minimizes the total projection error of the snapshots — with respect to the norm induced by \mathbf{X}_u — onto the column space of $\chi_{(1)}^u$ [27]. A common strategy consists in selecting n_u^s as the smallest integer N that satisfies the following relation:

$$\frac{\sum_{j=1}^N \sigma_j^2}{\sum_{j=1}^{N_\sigma} \sigma_j^2} \geq 1 - \epsilon_{POD}^2 \quad (3.7)$$

where $\epsilon_{POD} \in \mathbb{R}^+$ is a tolerance to be chosen *a priori*. The left-hand side of Eq.(3.7) represents the relative information (or energy) content of the POD basis.

Remark. Eq.(3.6) represents a huge SVD problem, that oftentimes is computationally prohibitive. However, we are only interested in performing a truncated SVD, i.e. in computing the $n_u^s \ll N_u^s$ most significant modes of $\mathbf{H}_u \chi_{(1)}^u$ and

the associated singular values. Such a task can be carried out at a reasonable computational cost exploiting iterative algorithms [28]. Moreover, optimized techniques to compute low-rank matrix approximations leveraging randomness could be employed, to further lighten the computational burden [29].

Among the possible strategies to compute the velocity reduced basis in time, we choose the *Fixed temporal subspace via T-HOSVD* one proposed in [2]. It simply consists in applying a “standard” (i.e. setting the norm matrix $\mathbf{X}_u^t = \mathbf{I}_{N^t}$) POD algorithm on the mode-2 unfolding of the snapshots’ tensor $\chi_{(2)}^u \in \mathbb{R}^{N^t \times N_u^s \times N_\mu}$. The number n_u^t of temporal reduced basis elements is chosen according to the criterion in Eq.(3.7) and the velocity temporal reduced basis is encoded in a matrix $\Psi^u \in \mathbb{R}^{N^t \times n_u^t}$, such that $(\Psi^u)^T \Psi^u = \mathbf{I}_{n_u^t}$.

In order to derive an expression for the spatio-temporal reduced basis, we assume that the FOM solution manifold $\mathcal{ST}_{h,\delta}^u$ can be well approximated by the low-dimensional vector space

$$\mathcal{ST}_{h,\delta}^u = \mathcal{S}_h^u \otimes \mathcal{T}_\delta^u \quad \text{with } \mathcal{S}_h^u = \text{span}\{\phi_i^u\}_{i=1}^{n_u^s} \text{ and } \mathcal{T}_\delta^u = \text{span}\{\psi_j^u\}_{j=1}^{n_u^t} \quad (3.8)$$

A generic element of the velocity space-time reduced basis can then be written as

$$\pi_{\mathcal{F}_u(i,j)}^u = \phi_i^u \otimes \psi_j^u \in \mathbb{R}^{N_u^s \times N^t} \quad i \in \{1, \dots, n_u^s\}, \quad j \in \{1, \dots, n_u^t\} \quad (3.9)$$

where $\mathcal{F}_u : (i, j) \mapsto (i-1)n_u^t + j$ is a bijective mapping from the space and time bases indexes to the space-time basis index and $\otimes : \mathbb{R}^N \times \mathbb{R}^M \rightarrow \mathbb{R}^{N \times M}$ (with $N, M \in \mathbb{N}$) denotes the outer product operator, i.e. $(\mathbf{u} \otimes \mathbf{v})_{ij} = \mathbf{u}_i \mathbf{v}_j$.

The same procedure applies for the assembling of the reduced bases of the other unknowns in Eq.(2.11), i.e. the pressure and the Lagrange multipliers. In particular:

- For the pressure, we assume that $\mathcal{ST}_{h,\delta}^p = \mathcal{S}_h^p \otimes \mathcal{T}_\delta^p$. We orthonormalize the reduced basis in space with respect to the $L^2(\Omega)$ -norm, which at discrete level is induced by the pressure mass matrix $\mathbf{M}_p \in \mathbb{R}^{N_p^s \times N_p^s}$ such that $(\mathbf{M}_p)_{ij} = \int_\Omega \varphi_j^p \varphi_i^p d\Omega$. We define the generic pressure space-time reduced basis element as

$$\pi_{\mathcal{F}_p(i,j)}^p = \phi_i^p \otimes \psi_j^p \in \mathbb{R}^{N_p^s \times N^t} \quad i \in \{1, \dots, n_p^s\}, \quad j \in \{1, \dots, n_p^t\} \quad (3.10)$$

with $\mathcal{F}_p : (i, j) \mapsto (i-1)n_p^t + j$. We denote the reduced basis in space by $\Phi^p \in \mathbb{R}^{N_p^s \times n_p^s}$ and the reduced basis in time by $\Psi^p \in \mathbb{R}^{N^t \times n_p^t}$.

- We compute a different reduced basis for each set of Lagrange multipliers, corresponding to different portions of $\tilde{\Gamma}_D$. So, for all $k \in \{1, \dots, N_D\}$, we define the spaces $\mathcal{ST}_{h,\delta}^{\lambda_k}$ such that $\mathcal{ST}_{h,\delta}^\lambda = \prod_{k=1}^{N_D} \mathcal{ST}_{h,\delta}^{\lambda_k}$ and we assume that $\mathcal{ST}_{h,\delta}^{\lambda_k} = \mathcal{S}_h^{\lambda_k} \otimes \mathcal{T}_\delta^{\lambda_k}$. As reduction in space is somehow already performed by discretizing the space \mathcal{L} as described in [18], we only have to compute N_D different temporal reduced bases. So, the generic space-time reduced basis element for the Lagrange multipliers associated to $\tilde{\Gamma}_D^k$ reads as:

$$\pi_{\mathcal{F}_{\lambda_k}(i,j)}^{\lambda_k} = \mathbf{e}_i \otimes \psi_j^{\lambda_k} \in \mathbb{R}^{N_\lambda^k \times N^t} \quad i \in \{1, \dots, N_\lambda^k\}, \quad j \in \{1, \dots, n_{\lambda_k}^t\} \quad (3.11)$$

where $\mathbf{e}_i \in \mathbb{R}^{N_\lambda^k}$ is the i -th canonical basis vector and $\mathcal{F}_{\lambda_k} : (i, j) \mapsto (i-1)n_{\lambda_k}^t + j$. We define the dimension of the space-time reduced basis as $n_{\lambda_k}^{st} := N_\lambda^k n_{\lambda_k}^t$. The space-time reduced basis for $\mathcal{ST}_{h,\delta}^\lambda$ can be then assembled exploiting the fact that $\mathcal{ST}_{h,\delta}^\lambda = \prod_{k=1}^{N_D} \mathcal{ST}_{h,\delta}^{\lambda_k}$ and its dimension is then equal to $n_\lambda^{st} = \sum_{k=1}^{N_D} n_{\lambda_k}^{st}$. We denote the reduced basis in space as $\Phi^\lambda = \mathbf{I}_{N_\lambda}$ — as no reduction in space takes place — and the reduced basis in time as $\Psi^\lambda = \text{diag}(\Psi^{\lambda_1}, \dots, \Psi^{\lambda_{N_D}}) \in \mathbb{R}^{N^t \times n_\lambda^t}$, with $n_\lambda^t := \sum_{k=1}^{N_D} n_{\lambda_k}^t$.

Ultimately, the global space-time reduced basis can be encoded in the matrix $\Pi \in \mathbb{R}^{N^{st} \times n^{st}}$ defined in Eq.(3.2), where $\Pi^u = \Phi^u \otimes \Psi^u$, $\Pi^p = \Phi^p \otimes \Psi^p$, $\Pi^\lambda = \mathbf{I}_{N_\lambda} \otimes \Psi^\lambda$.

3.3 Offline Phase: assembling of parameter-independent quantities

The second step of the offline phase consists in assembling, once and for all, the space-time reduced parameter-independent quantities. Problems featuring affine parametric dependency are considered in [30]; in the general case, approximate affine decompositions can be retrieved exploiting the (M)DEIM algorithm [31]. However, to simplify the analysis, in this work we restrict to the case when all parametric dependency comes with the Dirichlet data, whose information is stored in the right-hand side vector. Therefore, the reduced left-hand side matrix $\hat{\mathbf{A}}^{st}$ (see Eq.(2.11))

can be assembled once and for all at this stage. The computations can be performed efficiently, leveraging the saddle point structure of the matrix, so that

$$\hat{\mathbf{A}}^{st} = \begin{bmatrix} (\tilde{\mathbf{\Pi}}^u)^T \mathbf{A}_1^{st} \mathbf{\Pi}^u & (\tilde{\mathbf{\Pi}}^u)^T \mathbf{A}_2^{st} \mathbf{\Pi}^p & (\tilde{\mathbf{\Pi}}^u)^T \mathbf{A}_3^{st} \mathbf{\Pi}^\lambda \\ (\tilde{\mathbf{\Pi}}^p)^T \mathbf{A}_4^{st} \mathbf{\Pi}^u & & \\ (\tilde{\mathbf{\Pi}}^\lambda)^T \mathbf{A}_7^{st} \mathbf{\Pi}^u & & \end{bmatrix} = \begin{bmatrix} \hat{\mathbf{A}}_1^{st} & \hat{\mathbf{A}}_2^{st} & \hat{\mathbf{A}}_3^{st} \\ \hat{\mathbf{A}}_4^{st} & & \\ \hat{\mathbf{A}}_7^{st} & & \end{bmatrix}. \quad (3.12)$$

We refer to Eq.(2.12) for the definition of the FOM blocks $\{\mathbf{A}_i^{st}\}$. For the sake of simplicity, let us first consider a Galerkin projection, so $\tilde{\mathbf{\Pi}} = \mathbf{\Pi}$. In order to compute the 5 non-zero blocks of $\hat{\mathbf{A}}^{st}$, we can exploit the properties of the spatio-temporal reduced basis $\mathbf{\Pi}$. For instance, let us compute the value of $(\hat{\mathbf{A}}_1^{st})_{kl}$ for a generic couple of indexes $(k, l) \in \{1, \dots, n_u^{st}\} \times \{1, \dots, n_u^{st}\}$, such that $k = \mathcal{F}_u(k_s, k_t)$ and $l = \mathcal{F}_u(l_s, l_t)$, with $k_s, l_s \in \{1, \dots, n_u^s\}$, $k_t, l_t \in \{1, \dots, n_u^t\}$.

$$\begin{aligned} (\hat{\mathbf{A}}_1^{st})_{kl} &= (\mathbf{\pi}_k^u)^T \mathbf{A}_1^{st} \mathbf{\pi}_l^u = (\mathbf{\Phi}_{k_s}^u \otimes \mathbf{\Psi}_{k_t}^u)^T \mathbf{A}_4^{st} (\mathbf{\Phi}_{l_s}^u \otimes \mathbf{\Psi}_{l_t}^u) \\ &= (\mathbf{\Phi}_{k_s}^u \otimes \mathbf{\Psi}_{k_t}^u)^T \begin{bmatrix} \frac{1}{3} \mathbf{M} \phi_{l_s}^u(\psi_{l_t}^u)_1 & -\frac{4}{3} \mathbf{M} \phi_{l_s}^u(\psi_{l_t}^u)_1 & +(M + \frac{2}{3} \delta \mathbf{A}) \phi_{l_s}^u(\psi_{l_t}^u)_1 \\ \frac{1}{3} \mathbf{M} \phi_{l_s}^u(\psi_{l_t}^u)_2 & -\frac{4}{3} \mathbf{M} \phi_{l_s}^u(\psi_{l_t}^u)_2 & +(M + \frac{2}{3} \delta \mathbf{A}) \phi_{l_s}^u(\psi_{l_t}^u)_2 \\ \vdots & \vdots & \vdots \\ \frac{1}{3} \mathbf{M} \phi_{l_s}^u(\psi_{l_t}^u)_{N^t-2} & -\frac{4}{3} \mathbf{M} \phi_{l_s}^u(\psi_{l_t}^u)_{N^t-1} & +(M + \frac{2}{3} \delta \mathbf{A}) \phi_{l_s}^u(\psi_{l_t}^u)_{N^t} \end{bmatrix} \\ &= \left(\widehat{\mathbf{M}} + \frac{2}{3} \widehat{\mathbf{A}} \right)_{k_s l_s} \delta_{k_t, l_t} - \frac{4}{3} \widehat{\mathbf{M}}_{k_s l_s} (\psi_{k_t}^u)^T_{2:} (\psi_{l_t}^u)_{:N^t-1} + \frac{1}{3} \widehat{\mathbf{M}}_{k_s l_s} (\psi_{k_t}^u)^T_{3:} (\psi_{l_t}^u)_{:N^t-2} \end{aligned} \quad (3.13)$$

where $\widehat{\mathbf{M}} = (\mathbf{\Phi}^u)^T \mathbf{M} \mathbf{\Phi}^u$ is the space-reduced mass matrix and $\widehat{\mathbf{A}} = (\mathbf{\Phi}^u)^T \mathbf{A} \mathbf{\Phi}^u$ is the space-reduced stiffness matrix. Furthermore, $\delta_{i,j}$ is the Kronecker Delta function, which appears in Eq.(3.13) as the columns $\mathbf{\Psi}^u$ are orthonormal in Euclidean norm by construction, and the notations $v_{i:}$, $v_{:j}$ denote the sub-vector of a given vector \mathbf{v} containing all the entries from the i -th to the last and from the first to the j -th, respectively. A similar argument — actually simplified, as they are all block-diagonal — holds for the other four non-zero blocks of $\hat{\mathbf{A}}^{st}$. Thus, the assembly of the reduced left-hand side matrix only requires the spatial projection of the FOM matrices (see Eq.(2.6)) and some trivial multiplications between elements of the reduced bases in time. In particular, we define the space-reduced matrices

$$\begin{aligned} \widehat{\mathbf{A}} &= (\mathbf{\Phi}^u)^T \mathbf{A} \mathbf{\Phi}^u \in \mathbb{R}^{n_u^s \times n_u^s} & \widehat{\mathbf{B}}^T &= (\mathbf{\Phi}^u)^T \mathbf{B}^T \mathbf{\Phi}^p \in \mathbb{R}^{n_u^s \times n_p^s} & \widehat{\mathbf{B}} &= (\mathbf{\Phi}^p)^T \mathbf{B} \mathbf{\Phi}^u \in \mathbb{R}^{n_u^s \times n_p^s} \\ \widehat{\mathbf{M}} &= (\mathbf{\Phi}^u)^T \mathbf{M} \mathbf{\Phi}^u \in \mathbb{R}^{n_u^s \times n_u^s} & \widehat{\mathbf{C}}^T &= (\mathbf{\Phi}^u)^T \mathbf{C}^T \in \mathbb{R}^{n_u^s \times N_\lambda} & \widehat{\mathbf{C}} &= \mathbf{C} \mathbf{\Phi}^u \in \mathbb{R}^{N_\lambda \times n_u^s} \end{aligned} \quad (3.14)$$

and the following matrices, computed from the temporal reduced bases

$$\mathbf{\Psi}^{u,p} = (\mathbf{\Psi}^u)^T \mathbf{\Psi}^p \in \mathbb{R}^{n_u^t \times n_p^t} \quad \mathbf{\Psi}^{u,\lambda} = (\mathbf{\Psi}^u)^T \mathbf{\Psi}^\lambda \in \mathbb{R}^{n_u^t \times n_\lambda^t} \quad (3.15)$$

Then, the blocks of $\hat{\mathbf{A}}^{st}$ (other than $\hat{\mathbf{A}}_1^{st}$, already defined in Eq.(3.13)) read as:

$$\begin{aligned} \hat{\mathbf{A}}_2^{st} \in \mathbb{R}^{n_u^{st} \times n_p^{st}} : (\hat{\mathbf{A}}_2^{st})_{kl} &= \frac{1}{3} \delta \widehat{\mathbf{B}}_{k_s l_s}^T \mathbf{\Psi}_{k_t l_t}^{u,p} & \hat{\mathbf{A}}_4^{st} \in \mathbb{R}^{n_p^{st} \times n_u^{st}} : (\hat{\mathbf{A}}_4^{st})_{kl} &= \widehat{\mathbf{B}}_{k_s l_s} \mathbf{\Psi}_{k_t l_t}^{u,p} \\ \hat{\mathbf{A}}_3^{st} \in \mathbb{R}^{n_u^{st} \times n_\lambda^{st}} : (\hat{\mathbf{A}}_3^{st})_{kl} &= \frac{1}{3} \delta \widehat{\mathbf{C}}_{k_s l_s}^T \mathbf{\Psi}_{k_t l_t}^{u,\lambda} & \hat{\mathbf{A}}_7^{st} \in \mathbb{R}^{n_\lambda^{st} \times n_u^{st}} : (\hat{\mathbf{A}}_7^{st})_{kl} &= \widehat{\mathbf{C}}_{k_s l_s} \mathbf{\Psi}_{k_t l_t}^{u,\lambda} \end{aligned} \quad (3.16)$$

3.4 Online phase

During the online phase of the method, we are interested in computing the solution to the problem at hand for a given parameter value $\boldsymbol{\mu}^* \in \mathcal{D}$. This three steps:

1. The assembling of the reduced parameter-dependent quantities (i.e. the right-hand side vector)
2. The computation of the reduced solution
3. The reconstruction of an approximate FOM solution from the space-time reduced one

Concerning the first step, following Eq.(2.14), we just have to compute the third block of the right-hand side vector $\hat{\mathbf{F}}_3^{st}(\boldsymbol{\mu}^*) = (\mathbf{\Pi}^\lambda)^T \mathbf{F}_3^{st}(\boldsymbol{\mu}^*) \in \mathbb{R}^{n_\lambda^{st}}$. To this end, we can leverage the factorization of the Dirichlet datum in Eq.(2.13). The corresponding space-time reduced right-hand side $\hat{\mathbf{F}}_{3,k}^{st}(\boldsymbol{\mu}^*)$ is then given by

$$\hat{\mathbf{F}}_{3,k}^{st} = \hat{\mathbf{F}}_{3,k}^{st}(\boldsymbol{\mu}^*) \in \mathbb{R}^{n_{\lambda_k}^{st}} : (\hat{\mathbf{F}}_{3,k}^{st})_{\mathcal{F}_{\lambda_k}(i,j)} = (\tilde{\mathbf{g}}_k^s)_i \left((\psi_j^{\lambda_k})^T g^t(\boldsymbol{\mu}^*) \right) \quad (3.17)$$

Since the global space of Lagrange multipliers \mathcal{L} is such that $\mathcal{L} = \prod_{k=1}^{N_D} \mathcal{L}_k$, we have that

$$\widehat{\mathbf{F}}_3^{st}(\boldsymbol{\mu}^*) = \left[\left(\widehat{\mathbf{F}}_{3,1}^{st}(\boldsymbol{\mu}^*) \right)^T, \dots, \left(\widehat{\mathbf{F}}_{3,N_D}^{st}(\boldsymbol{\mu}^*) \right)^T \right]^T \in \mathbb{R}^{n_\lambda^{st}} \quad (3.18)$$

Notice that this assembling step is extremely cheap, as it only consists in performing N_D inner products between N^t -dimensional vectors.

Upon having assembled $\widehat{\mathbf{A}}^{st}$ (in the offline phase) and $\widehat{\mathbf{F}}_\mu^{st}$ (in the online phase), we are left with solving the n^{st} -dimensional dense linear system of Eq.(2.11). Since $n^{st} \ll N^{st}$, significant speedups with respect to the FOM can be attained.

Finally, once the space–time reduced solution $\hat{\mathbf{w}}(\boldsymbol{\mu}^*) \in \mathbb{R}^{n^{st}}$ is computed, it can be post–processed and re–projected onto the FOM space. This passage can be efficiently performed if the vector $\hat{\mathbf{w}}(\boldsymbol{\mu}^*) \in \mathbb{R}^{n^{st}}$ is suitably reshaped into a matrix $\hat{\mathbf{w}}^M(\boldsymbol{\mu}^*) \in \mathbb{R}^{n^s \times n^t}$, being $n^s = n_u^s + n_p^s + N_\lambda$ and $n^t = n_u^t + n_p^t + n_\lambda^t$. Indeed, the FOM reconstruction $\mathbf{w}_h^{st}(\boldsymbol{\mu}^*)$ of $\hat{\mathbf{w}}(\boldsymbol{\mu}^*)$ is as follows:

$$\mathbf{w}_h^{st}(\boldsymbol{\mu}^*) = \Phi \hat{\mathbf{w}}^M(\boldsymbol{\mu}^*) \Psi^T \in \mathbb{R}^{N^s \times N^t} \quad (3.19)$$

$\Phi := \text{diag}(\Phi^u, \Phi^p, \Phi^\lambda) \in \mathbb{R}^{N^s \times n^s}$ and $\Psi := \text{diag}(\Psi^u, \Psi^p, \Psi^\lambda) \in \mathbb{R}^{N^t \times n^t}$ are the global reduced bases in space and in time, respectively.

3.5 Definition of the norms

Concerning the spatial dimension, we already introduced the norms that we employed in Subsection 3.2 and we defined the corresponding matrices in Eq.(2.16).

Since temporal reduced bases are derived by imposing orthonormality in the Euclidean norm, we can define spatio–temporal norms as induced by the following matrices:

$$\mathbf{X}_u^{st} = \text{diag}\left(\underbrace{\mathbf{X}_u, \dots, \mathbf{X}_u}_{N^t}\right), \quad \mathbf{X}_p^{st} = \text{diag}\left(\underbrace{\mathbf{X}_p, \dots, \mathbf{X}_p}_{N^t}\right), \quad \mathbf{X}_\lambda^{st} = \text{diag}\left(\underbrace{\mathbf{X}_\lambda, \dots, \mathbf{X}_\lambda}_{N^t}\right). \quad (3.20)$$

The spatio–temporal norm matrix is then given by $\mathbf{X}^{st} = \text{diag}(\mathbf{X}_u^{st}, \mathbf{X}_p^{st}, \mathbf{X}_\lambda^{st}) \in \mathbb{R}^{N^{st} \times N^{st}}$.

In the reduced framework, the norms induced by the matrices in Eq.(2.16) can be efficiently computed, leveraging orthonormality. Indeed, since the reduced bases in space for velocity and pressure are orthonormal with respect to the norms induced by \mathbf{X}_u and \mathbf{X}_p respectively, we have that

$$\hat{\mathbf{X}}_u = (\Phi^u)^T \mathbf{X}_u \Phi^u = \mathbf{I}_{n_u^s}, \quad \hat{\mathbf{X}}_p = (\Phi^p)^T \mathbf{X}_p \Phi^p = \mathbf{I}_{n_p^s}, \quad \hat{\mathbf{X}}_\lambda = \mathbf{X}_\lambda = \mathbf{I}_{N_\lambda}. \quad (3.21)$$

Therefore, given $\bar{\mathbf{w}} = [\bar{\mathbf{u}}, \bar{\mathbf{p}}, \bar{\boldsymbol{\lambda}}] \in \mathbb{R}^{n_u^s + n_p^s + N_\lambda}$, the following holds:

$$\|\Phi^u \bar{\mathbf{u}}\|_{\mathbf{X}_u}^2 = \sum_{i,j=1}^{n_u^s} \bar{u}_i \bar{u}_j (\phi_i^u)^T \mathbf{X}_u \phi_j^u = \|\bar{\mathbf{u}}\|_2^2, \quad \|\Phi^p \bar{\mathbf{p}}\|_{\mathbf{X}_p}^2 = \sum_{i,j=1}^{n_p^s} \bar{p}_i \bar{p}_j (\phi_i^p)^T \mathbf{X}_p \phi_j^p = \|\bar{\mathbf{p}}\|_2^2 \quad (3.22)$$

Also, trivially, $\|\Phi_\lambda \bar{\boldsymbol{\lambda}}\|_{\mathbf{X}_\lambda}^2 = \|\bar{\boldsymbol{\lambda}}\|_2^2$. Following the same principle, since the reduced bases in time are orthonormal in ℓ^2 -norm and since we defined the spatio–temporal norms as induced by the matrices in Eq.(3.20), it holds that

$$\|\Pi^u \hat{\mathbf{u}}\|_{\mathbf{X}_u^{st}}^2 = \|\hat{\mathbf{u}}\|_2^2, \quad \|\Pi^p \hat{\mathbf{p}}\|_{\mathbf{X}_p^{st}}^2 = \|\hat{\mathbf{p}}\|_2^2, \quad \|\Pi^\lambda \hat{\boldsymbol{\lambda}}\|_{\mathbf{X}_\lambda^{st}}^2 = \|\hat{\boldsymbol{\lambda}}\|_2^2, \quad (3.23)$$

with $\hat{\mathbf{w}} = [\hat{\mathbf{u}}, \hat{\mathbf{p}}, \hat{\boldsymbol{\lambda}}] \in \mathbb{R}^{n_u^{st} + n_p^{st} + n_\lambda^{st}}$. Therefore, in the space–time reduced framework, the Euclidean norm is equivalent to the ones induced by the matrices in Eq.(3.20). This also means that the space–time reduced bases encoded by the matrices $\Pi^u, \Pi^p, \Pi^\lambda$ are orthonormal with respect to the inner product induced by the matrices in Eq.(3.20).

Finally, let us consider $\boldsymbol{\varphi}_j = \text{vec}(\phi_j \otimes \boldsymbol{\psi}_j) \in \mathbb{R}^{N^{st}}$ ($j \in \mathbb{N}$), being $\phi_j \in \mathbb{R}^{N^s}$ the vector of DOFs arising from the FE discretization of a spatial function $\phi_j = \phi_j(\mathbf{x})$ and $\boldsymbol{\psi}_j \in \mathbb{R}^{N^t}$ the vector storing the evaluations of a temporal function $\psi_j = \psi_j(t)$ at the equispaced time instants $\{t^k\}_{k=1}^{N^t}$ in $[0, T]$. Here $\text{vec} : \mathbb{R}^{N^s \times N^t} \rightarrow \mathbb{R}^{N^{st}}$ denotes the vectorization operator. Then, we have that:

$$(\boldsymbol{\varphi}_1, \boldsymbol{\varphi}_2)_{\mathbf{X}^{st}} = \sum_{k=1}^{N^t} (\phi_1(\boldsymbol{\psi}_1)_k, \phi_2(\boldsymbol{\psi}_2)_k)_{\mathbf{X}} = (\phi_1, \phi_2)_{\mathbf{X}} \sum_{k=1}^{N^t} (\boldsymbol{\psi}_1)_k (\boldsymbol{\psi}_2)_k \quad (3.24)$$

being $\mathbf{X}^{st} \in \mathbb{R}^{N^{st} \times N^{st}}$ a block-diagonal matrix constructed from the symmetric and positive definite norm matrix $\mathbf{X} \in \mathbb{R}^{N^s \times N^s}$, as the ones in Eq.(3.20). A consequence of Eq.(3.24) is that $(\varphi_j, \varphi_j)_{\mathbf{X}^{st}} = \|\varphi_j\|_{\mathbf{X}^{st}}^2 = \|\phi_j\|_{\mathbf{X}}^2 \|\psi_j\|_2^2$, so, the spatio-temporal norm factorizes into the product between the norms of the spatial and of the temporal factors. Incidentally, also Eq.(3.24) entails that the reduced bases encoded in the matrices $\mathbf{\Pi}^u, \mathbf{\Pi}^p, \mathbf{\Pi}^\lambda$ are orthonormal with respect to the norms induced by the matrices in Eq.(3.20).

3.6 Well-posedness of the ST-RB method

In Subsection 2.3, we highlighted that Problem 1 features a (twofold) saddle point structure and, as a consequence, it is associated with stability issues, related to the discretization of the spaces of the primal (velocity) and dual (pressure and Lagrange multipliers) fields. Assuming Problem 1 to be well-posed in the continuous setting, well-posedness in the discrete framework can be retained by satisfying the two *inf-sup* conditions in Eqs.(2.17a)-(2.17b). See Subsection 2.3 for details. However, even if a stable discretization is considered for the FOM, there is no guarantee for the *inf-sup* conditions to hold also for the reduced system (see e.g. [32, 33, 34, 35]). The literature presents several possibilities to deal with the loss of stability of saddle point problems in the context of model order reduction. In this work, we considered two of them, namely the supremizers enrichment [36, 30, 37] and the employment of least-squares Petrov-Galerkin reduced basis (LS-PG-RB) approaches for residual minimization [38, 39]. These two strategies lead to the development of the ST-GRB and ST-PGRB methods for unsteady parametrized incompressible Stokes equations, respectively.

3.6.1 Supremizers enrichment

The main idea of the supremizers enrichment approach is to augment the reduced basis for the velocity with additional elements (called *supremizers*) that are computed to ensure *inf-sup* stability also in the reduced framework. In particular, in order for the velocity reduced basis to be parameter-independent, in this work we perform an approximate supremizers enrichment [30]. To guarantee well-posedness, the two following *inf-sup* inequalities (reduced counterpart of Eq.(2.17b)) have to be satisfied:

$$\exists \beta_R > 0 : \inf_{\hat{\mathbf{q}} \neq \mathbf{0}} \sup_{\hat{\mathbf{v}} \neq \mathbf{0}} \frac{\hat{\mathbf{q}}^T \hat{\mathbf{B}} \hat{\mathbf{v}}}{\|\hat{\mathbf{v}}\|_2 \|\hat{\mathbf{q}}\|_2} \geq \beta_R \quad \text{and} \quad \inf_{\hat{\lambda} \neq \mathbf{0}} \sup_{\hat{\mathbf{v}} \neq \mathbf{0}} \frac{\hat{\lambda}^T \hat{\mathbf{C}} \hat{\mathbf{v}}}{\|\hat{\mathbf{v}}\|_2 \|\hat{\lambda}\|_2} \geq \beta_R \quad (3.25)$$

Here $\|\cdot\|_2$ denotes the Euclidean norm, which is identical to the ones induced by the matrices in Eq.(2.16) because of the orthonormality properties of the reduced bases (see subsection 3.2).

As the problem at hand features a twofold saddle point structure, two distinct sets of supremizers have to be computed. The first one — denoted as $\mathcal{S}_h^p := \{\mathbf{s}_j^{u,p}\}_{j=1}^{n_p^s}$ — is assembled by selecting, for each pressure mode ϕ_j^p , the velocity $\mathbf{s}_j^{u,p}$ that allows to attain the supremum in the pressure *inf-sup* inequality of Eq.(2.17b). Its elements are computed from the solutions to the following set of linear systems:

$$\begin{bmatrix} \mathbf{X}_u & \mathbf{C}^T \\ \mathbf{C} & \mathbf{0} \end{bmatrix} \begin{bmatrix} \mathbf{s}_j^{u,p} \\ \lambda_j \end{bmatrix} = \begin{bmatrix} \mathbf{B}^T \phi_j^p \\ \lambda_j \end{bmatrix} \quad \text{with } j \in \{1, \dots, n_p^s\} \quad (3.26)$$

We define $\mathcal{S}_h^{u,p+} = \text{span} \left\{ \{\phi_i^u\}_{i=1}^{n_u^s}, \{\mathbf{s}_j^{u,p}\}_{j=1}^{n_p^s} \right\}$ as the spatial reduced subspace for the velocity, enriched with pressure supremizers. The columns of the matrix $\Phi^{u,p+} = [\phi_1^u | \dots | \phi_{n_u^s}^u | \mathbf{s}_1^{u,p} | \dots | \mathbf{s}_{n_p^s}^{u,p}] \in \mathbb{R}^{N_u \times (n_u^s + n_p^s)}$ are then a basis of $\mathcal{S}_h^{u,p+}$.

Remark. Because of the twofold saddle point structure of the problem at hand, the computation of the pressure supremizers involves itself the numerical resolution of a saddle point problem, featuring $\mathbf{C} \in \mathbb{R}^{N_\lambda \times N_u^s}$ as constraint matrix. The primal solution $\mathbf{s}_j^{u,p}$ to such a problem satisfies the constraint $\mathbf{C} \mathbf{s}_j^{u,p} = \mathbf{0}$ (second equation of the system). Therefore, exploiting the first equation of the system, we have that $(\mathbf{s}_j^{u,p})^T \mathbf{B} \phi_j^p = (\mathbf{s}_j^{u,p})^T \mathbf{B} \phi_j^p - (\mathbf{s}_j^{u,p})^T \mathbf{C}^T \lambda_j = (\mathbf{s}_j^{u,p})^T \mathbf{X}_u \mathbf{s}_j^{u,p} = \|\mathbf{s}_j^{u,p}\|_{\mathbf{X}_u}^2$. This entails that, for the couple $(\mathbf{s}_j^{u,p}, \phi_j^p)$, the ratio in the pressure *inf-sup* condition reduces to $\|\mathbf{s}_j^{u,p}\|_{\mathbf{X}_u}$, as $\|\phi_j^p\|_{\mathbf{X}_p} = 1$ by construction. Thus, upon the proposed supremizers enrichment procedure, the well-posedness of the space-reduced problem can be empirically verified by assessing that $\exists \beta_R > 0 : \|\mathbf{s}_j^{u,p}\|_{\mathbf{X}_u} \geq \beta_R \quad \forall j \in \{1, \dots, n_p^s\}$.

The second set of supremizers is instead constructed from the bases of the spaces of Lagrange multipliers \mathcal{L}_h^k . It is now worth pointing out that the problem at hand actually features a $(N_D + 1)$ -fold saddle point structure, rather than a twofold one, as N_D distinct dual fields are defined to weakly impose inhomogeneous Dirichlet BCs. Therefore,

according to [19], the second *inf-sup* inequality in Eq.(2.17b) could be rewritten in terms of the local coupling matrices $\{C^k\}_{k=1}^{N_D}$ as follows:

$$\forall k \in \{1, \dots, N_D\} \quad \exists \beta_F^k > 0 : \quad \inf_{\lambda_k \neq 0} \sup_{\substack{\mathbf{v} \neq 0 \\ C^j \mathbf{v} = 0 \quad \forall j < k}} \frac{\lambda_k^T C^k \mathbf{v}}{\|\mathbf{v}\|_{\mathbf{X}_u} \|\lambda_k\|_{\mathbf{X}_{\lambda_k}}} \geq \beta_F^k \quad (3.27)$$

However, in the context of the problem at hand, Eq.(3.27) can be equivalently expressed as

$$\forall k \in \{1, \dots, N_D\} \quad \exists \beta_F^k > 0 : \quad \inf_{\lambda_k \neq 0} \sup_{\mathbf{v} \neq 0} \frac{\lambda_k^T C^k \mathbf{v}}{\|\mathbf{v}\|_{\mathbf{X}_u} \|\lambda_k\|_{\mathbf{X}_{\lambda_k}}} \geq \beta_F^k \quad (3.28)$$

provided that the inhomogeneous Dirichlet boundaries $\{\tilde{\Gamma}_D^k\}_{k=1}^{N_D}$ are disjoint. Therefore, for each $k \in \{1, \dots, N_D\}$, the Lagrange multipliers supremizers $\mathbf{s}_j^{u, \lambda_k}$ — with $j \in \{1, \dots, N_\lambda^k\}$ — are computed by solving the following linear systems:

$$\mathbf{X}_u \mathbf{s}_j^{u, \lambda_k} = C_k^T \mathbf{e}_j \quad \text{with } j \in \{1, \dots, N_\lambda^k\} \quad (3.29)$$

where $\mathbf{e}_j \in \mathbb{R}^{N_\lambda^k}$ is the j -th canonical basis element. The global set of Lagrange multipliers supremizers is then defined as $\mathcal{S}_h^\lambda := \{\mathbf{s}_j^{u, \lambda}\}_{j=1}^{N_\lambda} = \bigcup_{k=1}^{N_D} \left(\{\mathbf{s}_{j'}^{u, \lambda_k}\}_{j'=1}^{N_\lambda^k} \right)$ and we consider as spatial reduced subspace for the velocity $\mathcal{S}_h^{u, \lambda+} = \text{span} \left\{ \{\phi_i^u\}_{i=1}^{n_u^s}, \{\mathbf{s}_j^{u, \lambda}\}_{j=1}^{N_\lambda} \right\}$. A basis for such a subspace is represented by the columns of the matrix $\Phi^{u, \lambda+} = [\phi_1^u | \dots | \phi_{n_u^s}^u | \mathbf{s}_1^{u, \lambda} | \dots | \mathbf{s}_{N_\lambda}^{u, \lambda}] \in \mathbb{R}^{N_u^s \times (n_u^s + N_\lambda)}$.

Ultimately, we consider $\mathcal{S}_h^{u, p\lambda+} := \text{span} \left\{ \{\phi_i^u\}_{i=1}^{n_u^s}, \{\mathbf{s}_j^{u, p}\}_{j=1}^{n_p^s}, \{\mathbf{s}_j^{u, \lambda}\}_{j=1}^{N_\lambda} \right\}$ as reduced velocity subspace. An orthonormal basis — with respect to the norm induced by \mathbf{X}_u — for such a subspace is given by

$$\Phi^{u, p\lambda+} = [\phi_1^u | \dots | \phi_{n_u^s}^u | \phi_{n_u^s+1}^u | \dots | \phi_{n_u^s+n_p^s}^u | \phi_{n_u^s+n_p^s+1}^u | \dots | \phi_{n_u^s+n_p^s+N_\lambda}^u] \in \mathbb{R}^{N_u^s \times \tilde{n}_u^s} \quad (3.30)$$

where $\{\phi_{n_u^s+j}^u\}_{j=1}^{n_p^s}$ and $\{\phi_{n_u^s+n_p^s+j'}^u\}_{j'=1}^{N_\lambda}$ are computed from the solutions to Eqs.(3.26)-(3.29), applying the Gram-Schmidt algorithm and $\tilde{n}_u^s := n_u^s + n_p^s + N_\lambda$.

Remark. For the supremizers enrichment procedure, one could also consider the *inf-sup* condition in Eq.(2.17a), instead of the one in Eq.(2.17b). Under the assumption that the inhomogeneous Dirichlet boundaries are disjoint, this amounts at solving the following linear systems:

- *Pressure supremizers:* $\mathbf{X}_u \mathbf{s}_j^{u, p} = \mathbf{B}^T \phi_j^p$, with $j \in \{1, \dots, n_p^s\}$
- *Lagrange multipliers supremizers:* $\begin{bmatrix} \mathbf{X}_u & \mathbf{B}^T \\ \mathbf{B} & \end{bmatrix} \begin{bmatrix} \mathbf{s}_j^{u, \lambda_k} \\ \mathbf{q}_j \end{bmatrix} = \begin{bmatrix} C_k^T \mathbf{e}_j \\ \end{bmatrix}$, with $j \in \{1, \dots, N_\lambda^k\}$, $k \in \{1, \dots, N_D\}$.

Here $\mathbf{e}_j \in \mathbb{R}^{N_\lambda^k}$ denotes the j -th canonical basis vector.

However, with this approach, N_D saddle point problems featuring the matrix $\mathbf{B} \in \mathbb{R}^{N_p^s \times N_u^s}$ as constraint matrix have to be solved, instead of a single one, whose constraint is enforced via the “shorter” matrix $\mathbf{C} \in \mathbb{R}^{N_\lambda \times N_u^s}$ (as $N_\lambda \ll N_p^s$ in common applications).

When performing space–time model order reduction, the problem at hand preserves a twofold saddle point structure of type 1 (see Eq.(3.12)). In this context, the supremizers enrichment procedure of the velocity reduced basis in space is not enough to guarantee well-posedness. However, the following *inf-sup* inequalities hold, under the assumption that the matrices $\Psi^{u, p}$ and $\Psi^{u, \lambda}$ — defined in Eq.(3.15) — are full rank.

Lemma 1. *Let the velocity reduced basis in space be enriched with pressure supremizers \mathcal{S}_h^p . If the columns of the matrix $\Psi^{u, p}$ are linearly independent, then*

$$\exists \beta_{STR}^p > 0 \quad \text{such that} \quad \inf_{\hat{\mathbf{q}} \neq 0} \sup_{\substack{\hat{\mathbf{v}} \neq 0 \\ \hat{\mathbf{A}}_7^{st} \hat{\mathbf{v}} = 0}} \frac{\hat{\mathbf{q}}^T \hat{\mathbf{A}}_4^{st} \hat{\mathbf{v}}}{\|\hat{\mathbf{q}}\|_2 \|\hat{\mathbf{v}}\|_2} \geq \beta_{STR}^p \quad (3.31)$$

Proof. To satisfy Eq.(3.31), we need that $\exists \beta_{STR}^p > 0$ such that:

$$\forall \hat{\mathbf{q}} \neq \mathbf{0} \quad \exists \hat{\mathbf{v}} \neq \mathbf{0} \quad \text{such that} \quad \frac{\hat{\mathbf{q}}^T \hat{\mathbf{A}}_4^{st} \hat{\mathbf{v}}}{\|\hat{\mathbf{q}}\|_2 \|\hat{\mathbf{v}}\|_2} \geq \beta_{STR}^p \quad \text{and} \quad \hat{\mathbf{A}}_7^{st} \hat{\mathbf{v}} = \mathbf{0}$$

Let $vec_u : \mathbb{R}^{n_u^s \times n_u^t} \rightarrow \mathbb{R}^{n_u^s n_u^t}$ and $vec_p : \mathbb{R}^{n_p^s \times n_p^t} \rightarrow \mathbb{R}^{n_p^s n_p^t}$ be the vectorizing operators for velocity and pressure, respectively. Given $\hat{\mathbf{q}} = vec_p(\hat{\mathbf{q}}_s \otimes \hat{\mathbf{q}}_t) \in \mathbb{R}^{n_p^s n_p^t}$ and $\hat{\mathbf{v}} = vec_u(\hat{\mathbf{v}}_s \otimes \hat{\mathbf{v}}_t) \in \mathbb{R}^{n_u^s n_u^t}$, from the definition of $\hat{\mathbf{A}}_4^{st}$ (see Eq.(3.16)), we have that

$$\hat{\mathbf{q}}^T \hat{\mathbf{A}}_4^{st} \hat{\mathbf{v}} = \sum_{j=1}^{N^t} \left(\hat{\mathbf{q}}_s (\hat{\mathbf{q}}_t)_j \right)^T \hat{\mathbf{B}} \left(\hat{\mathbf{v}}_s (\hat{\mathbf{v}}_t)_j \right) = \sum_{j=1}^{N^t} (\hat{\mathbf{q}}_t)_j (\hat{\mathbf{v}}_t)_j \left(\hat{\mathbf{q}}_s^T \hat{\mathbf{B}} \hat{\mathbf{v}}_s \right) = (\hat{\mathbf{q}}_s^T \hat{\mathbf{B}} \hat{\mathbf{v}}_s) (\hat{\mathbf{q}}_t, \hat{\mathbf{v}}_t)_2 \quad (3.32)$$

where $(\hat{\mathbf{q}}_t)_j, (\hat{\mathbf{v}}_t)_j$ denote the j -th entry of $\hat{\mathbf{q}}_t, \hat{\mathbf{v}}_t$, respectively. Let us define $\hat{\mathbf{v}} := vec_u(\hat{\mathbf{s}}_s \otimes \hat{\mathbf{v}}_t)$, where $\hat{\mathbf{s}}_s$ is such that $\hat{\mathbf{C}} \hat{\mathbf{s}}_s = \mathbf{0}$ and $\hat{\mathbf{q}}_s^T \hat{\mathbf{B}} \hat{\mathbf{s}}_s \geq \beta_{RB}^p \|\hat{\mathbf{q}}_s\|_2 \|\hat{\mathbf{s}}_s\|_2$, with $\beta_{RB}^p > 0$. We have guarantee that $\hat{\mathbf{s}}_s$ exists, thanks to the supremizers enrichment procedure in space (see Eq.(3.26)). Firstly, we observe that $\hat{\mathbf{A}}_7^{st} \hat{\mathbf{v}} = \mathbf{0}$; indeed $(\hat{\mathbf{A}}_7^{st} \hat{\mathbf{v}})_k = (\hat{\mathbf{C}} \hat{\mathbf{s}}_s)_{k_s} \left((\Psi^{u,\lambda})^T \hat{\mathbf{v}}_t \right)_{k_t}$ (where $\mathcal{F}_\lambda(k_s, k_t) = k$, being \mathcal{F}_λ a suitably defined bijective index mapping) and $\hat{\mathbf{C}} \hat{\mathbf{s}}_s = \mathbf{0}$. So, the additional constraint appearing in the supremum of Eq.(3.31) is trivially satisfied. Then, considering Eq.(3.32), we have that

$$\hat{\mathbf{q}}^T \hat{\mathbf{A}}_4^{st} \hat{\mathbf{v}} = \left(\hat{\mathbf{q}}_s^T \hat{\mathbf{B}} \hat{\mathbf{s}}_s \right) (\hat{\mathbf{q}}_t, \hat{\mathbf{v}}_t)_2 \geq \beta_{RB}^p \|\hat{\mathbf{q}}_s\|_2 \|\hat{\mathbf{s}}_s\|_2 (\hat{\mathbf{q}}_t, \hat{\mathbf{v}}_t)_2$$

Therefore, as from Eq.(3.24) $\|\hat{\mathbf{q}}\|_2 = \|\hat{\mathbf{q}}_s\|_2 \|\hat{\mathbf{q}}_t\|_2$ and $\|\hat{\mathbf{v}}\|_2 = \|\hat{\mathbf{s}}_s\|_2 \|\hat{\mathbf{v}}_t\|_2$, we have that:

$$\frac{\hat{\mathbf{q}}^T \hat{\mathbf{A}}_4^{st} \hat{\mathbf{v}}}{\|\hat{\mathbf{q}}\|_2 \|\hat{\mathbf{v}}\|_2} \geq \beta_{RB}^p \frac{(\hat{\mathbf{q}}_t, \hat{\mathbf{v}}_t)_2}{\|\hat{\mathbf{q}}_t\|_2 \|\hat{\mathbf{v}}_t\|_2}$$

To conclude, Eq.(3.31) holds if $\exists \beta_t^p > 0$ such that

$$\forall \hat{\mathbf{q}}_t \neq \mathbf{0} \quad \exists \hat{\mathbf{v}}_t \neq \mathbf{0} \quad \text{such that} \quad \frac{(\hat{\mathbf{q}}_t, \hat{\mathbf{v}}_t)_2}{\|\hat{\mathbf{q}}_t\|_2 \|\hat{\mathbf{v}}_t\|_2} \geq \beta_t^p \quad (3.33)$$

This represents an *inf-sup* condition on the temporal reduced subspaces with respect to the Euclidean norm; based on the definition of the matrix $\Psi^{u,p}$ in Eq.(3.15), it is equivalent to the linear independence of the columns of $\Psi^{u,p}$. \square

Lemma 2. Let $k \in \{1, \dots, N_D\}$. Let the velocity reduced basis in space be enriched with Lagrange multipliers supremizers $S_h^{\lambda_k}$. If the columns of the matrix $\Psi^{u,\lambda_k} := (\Psi^u)^T \Psi^{\lambda_k}$ are linearly independent, then

$$\exists \beta_{STR}^{\lambda_k} > 0 \quad \text{such that} \quad \inf_{\hat{\lambda}_k \neq \mathbf{0}} \sup_{\hat{\mathbf{v}} \neq \mathbf{0}} \frac{\hat{\lambda}_k^T \left(\hat{\mathbf{A}}_7^{st} \right)^k \hat{\mathbf{v}}}{\|\hat{\lambda}_k\|_2 \|\hat{\mathbf{v}}\|_2} \geq \beta_{STR}^{\lambda_k} \quad (3.34)$$

where $\left(\hat{\mathbf{A}}_7^{st} \right)^k \in \mathbb{R}^{n_{st}^{\lambda_k} \times n_{st}^u}$ is the k -th block of $\hat{\mathbf{A}}_7^{st}$.

Proof. The proof proceeds as the one of Lemma 1. \square

Based on Lemmas 1 – 2, the following theorem concerning the well-posedness of the space-time-reduced problem holds.

Theorem 1. Let the velocity reduced basis in space be enriched with pressure supremizers S_h^p and Lagrange multipliers supremizers $S_h^{\lambda_k}$, computed solving Eqs.(3.26)–(3.29), respectively. Assume that the space-reduced problem is well-posed upon the supremizers enrichment procedure. If the columns of the matrices $\Psi^{u,p}, \Psi^{u,\lambda_k} \quad \forall k \in \{1, \dots, N_D\}$ are linearly independent, then the space-time-reduced problem arising from a Galerkin projection (Problem 2 with $\tilde{\Pi} = \Pi$) is well-posed.

Proof. The proof trivially follows from Lemmas 1 – 2, leveraging the assumption on the well-posedness of the space-reduced problem upon the supremizers enrichment procedure in space. \square

Algorithm 1 Temporal supremizers enrichment

```

1: function TEMPORALSUPREIMIZERS( $\Psi^u, \Psi^d, \epsilon_t$ ) ▷  $\Psi^d$  is the dual temporal basis matrix
2:   Compute  $\Psi^{u,d} = (\Psi^u)^T \Psi^d = [\xi_1 | \dots | \xi_{n_d^t}]$  ▷  $n_d^t$  is the number of dual temporal bases
3:   for  $\ell \in \{1, \dots, n_d^t\}$  do
4:     if  $\ell = 1$  then
5:        $\pi_\xi \leftarrow \xi_1$ 
6:     else
7:        $\pi_\xi \leftarrow \sum_{j=1}^{\ell-1} \frac{(\xi_\ell, \xi_j)_2}{(\xi_j, \xi_j)_2} \xi_j$  ▷ Compute the projection of  $\xi_\ell$  onto  $\text{span}\{\xi_j\}_{j=1}^{\ell-1}$ 
8:     end if
9:     if  $\|\xi_\ell - \pi_\xi\|_2 \leq \epsilon_t$  then ▷ Check enrichment condition
10:       $\psi^* \leftarrow \Psi_{:, \ell}^d$ 
11:       $\psi^+ = \left( \psi^* - \sum_{j=1}^{n_u^t} (\psi^*, \psi_j^u)_2 \psi_j^u \right) / \left\| \psi^* - \sum_{j=1}^{n_u^t} (\psi^*, \psi_j^u)_2 \psi_j^u \right\|_2$ 
12:       $\Psi^u \leftarrow [\Psi^u | \psi^+]$  ▷ Enrich velocity temporal reduced basis
13:       $n_u^t \leftarrow n_u^t + 1$ 
14:       $\Psi^{u,d} = [\xi_1 | \dots | \xi_{n_p^t}] \leftarrow \left[ (\Psi^{u,d})^T \mid ((\psi^+)^T \Psi^d)^T \right]^T$  ▷ Update  $\Psi^{u,d}$ 
15:       $\ell \leftarrow 1$ 
16:    else
17:       $\xi_\ell \leftarrow \xi_\ell - \pi_\xi$ 
18:    end if
19:  end for
20: end function

```

As the temporal reduced bases for velocity, pressure and Lagrange multipliers have been derived independently, we do not have any guarantee that the matrices $\Psi^{u,p}$ and $\{\Psi^{u,\lambda_k}\}_{k=1}^{N_D}$ are indeed full column rank. In order for the *inf-sup* inequalities in Eqs.(3.31)-(3.34) to be satisfied it is necessary to extend the supremizers enrichment procedure also to the temporal reduced basis of the velocity.

Corollary 1. *Let the velocity reduced basis in space be enriched with pressure supremizers S_h^p . Assume that the columns of $\Psi^{u,p}$ are linearly dependent. If the velocity temporal reduced basis Ψ^u is enriched according to Algorithm 1, setting $\Psi^d = \Psi^p$ and fixing $\epsilon_t \geq 0$, then the *inf-sup* inequality in Eq.(3.31) is satisfied.*

Proof. Let us denote the columns of $\Psi^{u,p}$ as $\{\xi_\ell\}_{\ell=1}^{n_p^t}$. Since the elements of $\{\xi_\ell\}_{\ell=1}^{n_p^t}$ are linearly dependent, $\exists \bar{\alpha} = [\bar{\alpha}_1, \dots, \bar{\alpha}_{n_p^t}] \neq \mathbf{0}$ such that

$$\vartheta := \sum_{\ell=1}^{n_p^t} \bar{\alpha}_\ell \xi_\ell = \sum_{\ell=1}^{n_p^t} \bar{\alpha}_\ell (\Psi^u)^T \psi_\ell^p = \mathbf{0} \in \mathbb{R}^{n_u^t} \quad (3.35)$$

The goal is to enrich the temporal velocity reduced basis in such a way that Eq.(3.35) cannot hold and it can be accomplished applying Algorithm 1, with pressure as dual field. So, let us set $\Psi^d = \Psi^p$ and let $\epsilon_t \geq 0$ (Line 1). We proceed iteratively, showing that, upon a suitable enrichment procedure, $\forall \ell^* \in \{1, \dots, n_p^t\}$, $\nexists \bar{\alpha} = [\bar{\alpha}_1, \dots, \bar{\alpha}_{\ell^*}] \in \mathbb{R}^{\ell^*}$, $\bar{\alpha} \neq \mathbf{0}$ such that

$$\vartheta := \sum_{\ell=1}^{\ell^*} \bar{\alpha}_\ell \xi_\ell = \sum_{\ell=1}^{\ell^*} \bar{\alpha}_\ell (\Psi^u)^T \psi_\ell^p = \mathbf{0} \in \mathbb{R}^{n_u^t} \quad (3.36)$$

Firstly, let us consider the case $\ell^* = 1$. So, suppose that $\xi_1 = \mathbf{0}$, so that $\|\xi_1\|_2 \leq \epsilon_t \forall \epsilon_t \geq 0$. This means that the first pressure temporal basis function ψ_1^p belongs to the orthogonal complement of the velocity temporal reduced subspace. In such a case, $\Psi^{u,p}$ cannot be full column rank and any $\bar{\alpha} = [\bar{\alpha}_1] \in \mathbb{R}^1$ trivially satisfies Eq.(3.36). Let us now enrich the velocity temporal reduced basis with ψ_1^p (Lines 11–12). Upon the enrichment, the last entry of ξ_1 equals $(\psi_1^p, \psi_1^p)_2 = \|\psi_1^p\|_2^2 = 1$, so $\xi_1 \neq \mathbf{0}$. Hence, for $\ell^* = 1$ Eq.(3.36) is satisfied and by Lemma 1 *inf-sup* stability with respect to the space spanned by ψ_1^p is attained.

Let us now consider $\ell^* \in \{2, \dots, n_p^t\}$ and let us suppose that Eq.(3.36) holds for $\ell^* - 1$. Let $\Psi^u \in \mathbb{R}^{N^t \times n_u^t}$ be the matrix encoding the temporal velocity reduced basis at the ℓ^* -th step of the algorithm; notice that the value of n_u^t may

have changed during the application of the algorithm. Let also $\Psi^{u,p} = (\Psi^u)^T \Psi^p = [\xi_1 | \dots | \xi_{n_p^t}] \in \mathbb{R}^{n_u^t \times n_p^t}$. If the first ℓ^* columns of $\Psi^{u,p}$ are linearly independent, then Eq.(3.36) holds by definition and via Lemma 1 *inf-sup* stability with respect to the space spanned by $\{\psi_j^p\}_{j=1}^{\ell^*}$ is guaranteed. Otherwise, ξ_{ℓ^*} can be expressed as a linear combination of the previous elements $\{\xi_\ell\}_{\ell=1}^{\ell^*-1}$. Such a condition can be verified by comparing ξ_{ℓ^*} with its orthogonal projection $\pi_{\xi_{\ell^*}}$ onto the $(\ell^* - 1)$ -dimensional subspace spanned by $\{\xi_\ell\}_{\ell=1}^{\ell^*-1}$. Indeed, if Eq.(3.36) does not hold, then ξ_{ℓ^*} is such that $\|\xi_{\ell^*} - \pi_{\xi_{\ell^*}}\|_2 = 0$ and so $\|\xi_{\ell^*} - \pi_{\xi_{\ell^*}}\|_2 \leq \epsilon_t \forall \epsilon_t \geq 0$ (Lines 7–9). In this case, we enrich the velocity temporal reduced basis with the pressure temporal basis function $\psi_{\ell^*}^p$ associated to ξ_{ℓ^*} , i.e. $\xi_{\ell^*} = (\Psi^u)^T \psi_{\ell^*}^p$ (Lines 11–12). We have to verify that, upon the enrichment procedure, Eq.(3.36) holds for the current value of ℓ^* . Let us consider the last entry of ϑ , that corresponds to the novel velocity temporal basis function $\psi_{n_u^t+1}^u = \psi_{\ell^*}^p$. Exploiting the orthonormality of the pressure temporal basis functions, we have that

$$(\vartheta)_{n_u^t+1} = \sum_{\ell=1}^{\ell^*} \bar{\alpha}_\ell (\xi_\ell)_{n_u^t+1} = \sum_{\ell=1}^{\ell^*} \bar{\alpha}_\ell (\psi_{\ell^*}^p, \psi_\ell^p)_2 = \sum_{\ell=1}^{\ell^*} \bar{\alpha}_\ell \delta_{\ell\ell^*} = \bar{\alpha}_{\ell^*} = 0 \implies \bar{\alpha}_{\ell^*} = 0$$

Therefore, $\bar{\alpha}_{\ell^*} = 0$ and Eq.(3.36) reduces to $\vartheta = \sum_{\ell=1}^{\ell^*-1} \bar{\alpha}_\ell \xi_\ell = \mathbf{0}$. However, since the first n_u^t components of the vectors $\{\xi_\ell\}_{\ell=1}^{\ell^*-1}$ are linearly independent by hypothesis, we also have that $\bar{\alpha}_\ell = 0 \forall \ell \in \{1, \dots, \ell^* - 1\}$. So, Eq.(3.36) is satisfied for the current value of ℓ^* and, upon the supremizers enrichment, the first ℓ^* columns of $\tilde{\Psi}^{u,p}$ are linearly independent.

Proceeding by induction up to $\ell^* = n_p^t$, we can then prove that, upon the supremizers enrichment procedure described in Algorithm 1, Eq.(3.35) cannot hold. Therefore, the *inf-sup* inequality in Eq.(3.31) is satisfied.

One remark is necessary in order to conclude the proof. In Line 14 of Algorithm 1, the velocity temporal reduced basis is not enriched with the “critical” pressure basis function $\psi_{\ell^*}^p$ (as we assumed before), but with the normalized orthogonal complement ψ^+ of the latter with respect to the space spanned by $\{\psi_j^u\}_{j=1}^{n_u^t}$ (Line 11). In this way, the velocity temporal reduced basis remains orthonormal even upon the enrichment procedure. However, this does not impact the linear independence of the columns of $\Psi^{u,p}$, since the subspaces spanned by $\{\{\psi_j^u\}_{j=1}^{n_u^t}, \psi_{\ell^*}^p\}$ and by $\{\{\psi_j^u\}_{j=1}^{n_u^t}, \psi^+\}$ trivially coincide. \square

Remark. The choice $\epsilon_t = 0$ is enough to retain *inf-sup* stability as it guarantees that β_t^p in Eq.(3.33) is strictly positive. However, if the columns of $\Psi^{u,p}$ are “almost” collinear, then $\beta_t^p \gtrsim 0$ and the accuracy of the method is compromised. Hence, from a numerical standpoint, selecting $\epsilon_t > 0$ is crucial. We numerically investigated the effect of ϵ_t in Subsection 4.2.

Corollary 2. *Let $k \in \{1, \dots, N_D\}$. Let the velocity reduced basis in space be enriched with the k -th Lagrange multiplier supremizers $S_h^{\lambda_k}$. Assume that the columns of Ψ^{u,λ_k} are linearly dependent. If the velocity temporal reduced basis Ψ^u is enriched according to Algorithm 1, setting $\Psi^d = \Psi^{\lambda_k}$ and fixing $\epsilon_t \geq 0$, then the *inf-sup* inequality in Eq.(3.34) is satisfied.*

Proof. The proof proceeds as the one of Corollary 1, taking advantage of Lemma 2. \square

Therefore, under the assumption that the space-reduced problem is well-posed upon a suitable supremizers enrichment procedure, the space-time-reduced problem arising from a Galerkin projection is also well-posed if the velocity temporal reduced basis is enriched according to Corollaries 1 – 2. A remark is worth to follow. While supremizers enrichment in space has to be performed with respect to all the dual fields in order to guarantee *inf-sup* stability, in time we can often consider only one of them. Indeed, once the velocity temporal reduced basis has been enriched with supremizers associated, say, to pressure (so that $\Psi^{u,p}$ is full column rank), it is often the case that also the columns of the matrices Ψ^{u,λ_k} (with $k \in \{1, \dots, N_D\}$) are linearly independent. If so, no further supremizers enrichment along the temporal dimension is necessary. As a consequence, the “stabilized” velocity temporal reduced basis depends on the order in which the supremizers are added. We numerically investigated this aspect in Subsection 4.2.

3.6.2 Least-squares Petrov–Galerkin projection

Least-squares (LS) Petrov–Galerkin (PG) reduced basis (RB) methods (hereafter referred to as LS-PG-RB) have already been proposed in the framework of space-time model order reduction in [2, 17]. The main idea of such methods is to minimize the FOM residual $\mathbf{r}_\mu^{st}(\hat{\mathbf{w}}) := \mathbf{F}_\mu^{st} - \mathbf{A}^{st} \Pi \hat{\mathbf{w}}$, evaluated in the full-order reconstruction of the space-time

reduced solution. Since $\hat{\mathbf{w}} \in \mathbb{R}^{n^{st}}$ and $n^{st} \ll N^{st}$, the system $\mathbf{r}_\mu^{st}(\hat{\mathbf{w}}) = \mathbf{0}$ is over-determined. In [2], a solution is computed by solving the following minimization problem:

$$\text{Find } \hat{\mathbf{w}} \in \mathbb{R}^{n^{st}} \text{ such that } \hat{\mathbf{w}} = \underset{\hat{\mathbf{v}} \in \mathbb{R}^{n^{st}}}{\operatorname{argmin}} \frac{1}{2} \|\mathbf{r}_\mu^{st}(\hat{\mathbf{v}})\|_{\mathbf{W}^T \mathbf{W}}^2 \quad (3.37)$$

where $\mathbf{W} \in \mathbb{R}^{n_w \times N^{st}}$ (with $n_w \geq n^{st}$ in order for the resulting linear system to be non-singular) is a space-time weighting matrix. Different approaches for the assembly of \mathbf{W} are discussed and some non-linear 1D problems are investigated.

In this work, we decided to extend the LS-PG-RB method, proposed for steady parametrized Stokes equations in [40, 38], to the time-dependent case, in the framework of space-time model order reduction. In the steady case, the key idea of the method is to define a global parameter-dependent supremizing operator $T^\mu : \mathcal{S}_h \rightarrow \mathcal{S}_h$ such that

$$(T^\mu(\underline{z}_h), \underline{w}_h)_{\mathcal{S}_h} = \mathcal{A}^\mu(\underline{z}_h, \underline{w}_h) \quad (3.38)$$

where \mathcal{S}_h is the finite-dimensional subspace where the FOM solutions are sought, equipped with the inner product $(\cdot, \cdot)_{\mathcal{S}_h}$, and \mathcal{A}^μ is the global parameter-dependent steady Stokes operator. Then, the LS-PG-RB method stems from a Petrov-Galerkin projection, where the trial subspace $\mathcal{S}_n := \operatorname{span} \{\xi_i, i \in \{1, \dots, n\}\} \subset \mathcal{S}_h$ is computed in a standard fashion (e.g. by truncated POD of the mode-1 unfolding of the snapshots tensor), while the test one is defined as $\tilde{\mathcal{S}}_n := \operatorname{span} \{T^\mu(\xi_i), i \in \{1, \dots, n\}\}$. From an algebraic standpoint, the basis of the test space can be encoded in the matrix $\mathbf{X}_h^{-1} \mathbf{A}_h^\mu \Phi \in \mathbb{R}^{N^s \times N^s}$, where $\mathbf{X}_h \in \mathbb{R}^{N^s \times N^s}$ is the FOM norm matrix, $\mathbf{A}_h^\mu \in \mathbb{R}^{N^s \times N^s}$ is the FOM discretization of the global steady Stokes operator and $\Phi \in \mathbb{R}^{N^s \times n^s}$ is the matrix encoding the reduced basis. Ultimately, the solution is retrieved by solving the following linear system

$$\begin{aligned} \mathbf{A}_n^\mu \mathbf{w}_n &= \mathbf{f}_n^\mu \quad \text{with} \quad \mathbf{A}_n^\mu = (\mathbf{A}_h^\mu \Phi)^T \mathbf{X}_h^{-1} \mathbf{A}_h^\mu \Phi \in \mathbb{R}^{n^s \times n^s} \\ \mathbf{f}_n^\mu &= (\mathbf{A}_h^\mu \Phi)^T \mathbf{X}_h^{-1} \mathbf{f}_h^\mu \in \mathbb{R}^{n^s} \end{aligned} \quad (3.39)$$

where $\mathbf{f}_h^\mu \in \mathbb{R}^{N^s}$ is the parameter-dependent FOM right-hand side. A key property of the LS-PG-RB method is that the choice of the test space $\tilde{\mathcal{S}}_n$ automatically guarantees *inf-sup* stability. Therefore, no supremizers enrichment procedure of the velocity reduced basis has to be performed to retain well-posedness. Additionally, it can be shown that the solution to Eq.(3.39) minimizes the FOM residual in the norm induced by \mathbf{X}_h^{-1} . We refer to [40, 27] for further details.

In [38], the authors present a purely algebraic LS-PG-RB method, based on the substitution of the norm matrix \mathbf{X}_h with a suitable surrogate \mathbf{P}_X . This provides significant computational gains if parametrized geometries are considered. Indeed, in such cases, the norm matrix \mathbf{X}_h is parameter-dependent and the computation of its inverse during the online phase of the method (to assemble \mathbf{A}_n^μ and \mathbf{f}_n^μ) may well represent a computational bottleneck. A smart choice consists then in choosing the surrogate \mathbf{P}_X as an easy-to-invert and parameter-independent matrix.

Focusing on the problem at hand and in the context of space-time model order reduction, the application of the LS-PG-RB method amounts at solving the following minimization problem:

$$\text{Find } \hat{\mathbf{w}}^{pg} \in \mathbb{R}^{n^{st}} \text{ such that: } \hat{\mathbf{w}}^{pg} = \underset{\hat{\mathbf{v}} \in \mathbb{R}^{n^{st}}}{\operatorname{argmin}} \frac{1}{2} \|\mathbf{r}_\mu^{st}(\hat{\mathbf{v}})\|_{(\mathbf{X}^{st})^{-1}}^2 \quad (3.40)$$

We refer to Eq.(3.40) as the ST-PGRB problem. Exploiting the convexity of the functional to be minimized, $\hat{\mathbf{w}}$ can be computed as the solution of the following linear system:

$$\begin{aligned} \hat{\mathbf{A}}^{pg} \hat{\mathbf{w}}^{pg} &= \hat{\mathbf{F}}_\mu^{pg} \quad \text{with} \quad \hat{\mathbf{A}}^{pg} = (\mathbf{A}^{st} \Pi)^T (\mathbf{X}^{st})^{-1} \mathbf{A}^{st} \Pi \in \mathbb{R}^{n^{st} \times n^{st}} \\ \hat{\mathbf{F}}_\mu^{pg} &= (\mathbf{A}^{st} \Pi)^T (\mathbf{X}^{st})^{-1} \mathbf{F}_\mu^{st} \in \mathbb{R}^{n^{st}} \end{aligned} \quad (3.41)$$

The block structure of the problem at hand can be exploited to ease the assembling of $\hat{\mathbf{A}}^{pg}$ and $\hat{\mathbf{F}}_\mu^{pg}$. We refer to Appendix A for all the details. By analogy with the steady case (see Eq.(3.38)), we can define a space-time global supremizing operator $\mathcal{T}^{st} : \mathcal{ST}_{h,\delta} \rightarrow \mathcal{ST}_{h,\delta}$ such that

$$(\mathcal{T}^{st}(\underline{z}_{h,\delta}), \underline{w}_{h,\delta})_{\mathcal{ST}_{h,\delta}} = \mathcal{A}^{st}(\underline{z}_{h,\delta}, \underline{w}_{h,\delta}) \quad (3.42)$$

where \mathcal{A}^{st} a bilinear form corresponding to the space-time global Stokes operator, whose full-order algebraic counterpart is given by the matrix \mathbf{A}^{st} , defined in Eq.(2.11). Notice that, since \mathcal{A}^{st} does not depend on the parameters, neither the global supremizing operator does. From an algebraic standpoint, the basis of the test space — constructed as orthonormal with respect to the norm induced by \mathbf{X}^{st} (see Eq.(3.20)) — can be encoded in the matrix $\tilde{\Pi} = (\mathbf{X}^{st})^{-1} \mathbf{A}^{st} \Pi \in \mathbb{R}^{N^{st} \times n^{st}}$.

Theorem 2. Assume that the conditions in Eq.(2.17a) hold. Define $\tilde{\Pi} := (\mathbf{X}^{st})^{-1} \mathbf{A}^{st} \Pi$. Then, the ST-PGRB problem in Eq.(3.40) is *inf-sup stable*, i.e.

$$\exists \beta_{STPG} > 0 \quad \text{such that} \quad \inf_{\hat{\mathbf{w}} \neq \mathbf{0}} \sup_{\hat{\mathbf{y}} \neq \mathbf{0}} \frac{\hat{\mathbf{w}}^T \hat{\mathbf{A}}^{pg} \hat{\mathbf{y}}}{\|\hat{\mathbf{w}}\|_2 \|\hat{\mathbf{y}}\|_2} \geq \beta_{STPG} \quad (3.43)$$

Moreover, the problem admits a unique solution $\hat{\mathbf{w}}^{pg}(\boldsymbol{\mu}) \in \mathbb{R}^{n^{st}}$ for every $\boldsymbol{\mu} \in \mathcal{D}$ that satisfies

$$\|\hat{\mathbf{w}}^{pg}(\boldsymbol{\mu})\|_2 \leq \frac{1}{\beta_{STPG}} \|\mathbf{F}_{\boldsymbol{\mu}}^{st}\|_{(\mathbf{X}^{st})^{-1}} \quad (3.44)$$

We refer to [40, 27] for the proof of a corresponding result in the steady case. Upon defining the global supremizing operator as in Eq.(3.42), the same proof applies to the time-dependent case, leveraging space-time model order reduction.

Remark. Even if we did not focus on problems featuring parametrized geometries, we anyway decided to approximate the spatio-temporal norm matrix \mathbf{X}^{st} with an easy-to-invert surrogate $\mathbf{P}_{\mathbf{X}}$, defined as its diagonal part, so that $(\mathbf{P}_{\mathbf{X}})_{ij} = (\mathbf{X}^{st})_{ij} \delta_{ij}$. If there exist two positive constants c, C — with $c \leq C$ — so that

$$c \|\mathbf{w}\|_{\mathbf{P}_{\mathbf{X}}} \leq \|\mathbf{w}\|_{\mathbf{X}^{st}} \leq C \|\mathbf{w}\|_{\mathbf{P}_{\mathbf{X}}} \quad \forall \mathbf{w} \in \mathbb{R}^{N^{st}} \quad (3.45)$$

then the ST-PGRB problem featuring $\mathbf{P}_{\mathbf{X}}$ as (approximate) spatio-temporal norm matrix is *inf-sup stable* and its *inf-sup* stability constant is $\tilde{\beta}_{STPG} = \frac{c}{C} \beta_{STPG}$, with β_{STPG} defined as in Theorem 2. The proof of a corresponding result in the steady case can be found in [38] and its extension to the unsteady case is straightforward.

4 Experimental results

We considered two different ST-RB methods, namely

1. *ST-GRB*: method stemming from a Galerkin projection onto a suitably computed spatio-temporal low-dimensional subspace. The velocity reduced bases (in space and in time) are enriched with supremizers in order to retain *inf-sup* stability (see Subsection 3.6.1).
2. *ST-PGRB*: method stemming from the minimization of the spatio-temporal FOM residual in the norm induced by the inverse of the spatio-temporal norm matrix \mathbf{X}^{st} . No supremizers enrichment is necessary, neither in space nor in time, as this formulation is equivalent to a Petrov–Galerkin projection, where the test space is conveniently defined in order to “automatically” retain *inf-sup* stability (see Subsection 3.6.2).

Additionally, we took the “standard” RB method (denoted as SRB-TFO), featuring dimensionality reduction only in space by means of a Galerkin projection, as a baseline. Supremizers enrichment (in space) is necessary to retain *inf-sup* stability (see Eq.(2.17a)).

4.1 Setup

We solved the unsteady incompressible Stokes equations (see Eq.(2.1)) in two different geometries: (1) an idealized symmetric bifurcation with characteristic angle $\alpha = 50^\circ$; (2) a patient-specific geometry of a femoropopliteal bypass (see Figure 1) The geometries of the bifurcation is identical to the one employed in [18] as building block for the modular geometrical approximation of blood vessels. The geometry of the femoropopliteal bypass — bridging the circulation between the femoral artery and the popliteal one in case of severe stenotic formations in the former — has been reconstructed from CT scans as detailed in [41] and it has been employed e.g. in [42, 43]. For all the simulations, we fixed $\rho = 1.06 \text{ g} \cdot \text{cm}^{-3}$ and $\mu = 3.5 \cdot 10^{-3} \text{ g} \cdot \text{cm}^{-1} \cdot \text{s}^{-1}$. As shown in Eq.(2.13), we considered the parametric dependency to exclusively characterize the temporal part of the Dirichlet datum g^μ . In particular, we designed g^μ in order to impose T -periodic parabolic velocity profiles at the boundaries belonging to $\tilde{\Gamma}_D$, being T the final time of the simulation. So, let us introduce the function $g_{ref}^\mu : \Gamma \times [0, T] \rightarrow \mathbb{R}$ — being Γ a circular surface of radius R and center \mathbf{x}_0 — such that $g_{ref}^\mu(\mathbf{x}, t) = g_{ref}^s(\mathbf{x}) g_{ref}^t(t; \boldsymbol{\mu})$. We define

$$\begin{aligned} g_{ref}^s(\mathbf{x}) &:= \frac{2}{\pi R^2} \left(1 - \frac{\|\mathbf{x} - \mathbf{x}_0\|^2}{R^2} \right) & \mathbf{x} \in \Gamma \\ g_{ref}^t(t; \boldsymbol{\mu}) &:= 1 - \cos \frac{2\pi t}{T} + \mu_1 \sin \frac{2\pi \mu_0 t}{T} & t \in [0, T] \end{aligned} \quad (4.1)$$

The Dirichlet datum is then defined as follows in the two test cases:

geometry	n° elements		n° vertices	
	domain tetrahedra	boundary triangles	P1	P2
Bifurcation	16844	3422	3552	25658
Bypass	55456	5082	10158	78312

Table 1. Number of elements (volume tetrahedra and boundary triangles) and number of and vertices (P1 and P2) relative to the employed computational meshes

- **Symmetric Bifurcation:** we impose a parametrized T -periodic parabolic velocity profile at the inlet and we prescribe the flow rate in one of the outlets, expressed as a given percentage of the inflow rate. So,

$$\underline{g}^\mu(\mathbf{x}, t) := \begin{cases} \underline{g}_{ref}^\mu(\mathbf{x}, t) & (\mathbf{x}, t) \in \Gamma_{IN}^1 \times [0, T] \\ \mu_2 \underline{g}_{ref}^\mu(\mathbf{x}, t) & (\mathbf{x}, t) \in \Gamma_{OUT}^1 \times [0, T] \end{cases} \quad (4.2)$$

with $\mu \in \mathcal{D} := [4, 8] \times [0.1, 0.3] \times [0.2, 0.8]$. On the other outlet Γ_{OUT}^2 we impose homogeneous Neumann BCs.

- **Femoropopliteal Bypass:** we impose two different T -periodic parabolic velocity profiles on the two inlets, constraining their sum to be constant and equal to \underline{g}_{ref}^μ , i.e.

$$\underline{g}^\mu(\mathbf{x}, t) := \begin{cases} \mu_2 \underline{g}_{ref}^\mu(\mathbf{x}, t) & (\mathbf{x}, t) \in \Gamma_{IN}^1 \times [0, T] \\ (1 - \mu_2) \underline{g}_{ref}^\mu(\mathbf{x}, t) & (\mathbf{x}, t) \in \Gamma_{IN}^2 \times [0, T] \end{cases} \quad (4.3)$$

with $\mu \in \mathcal{D} := [4, 8] \times [0.1, 0.3] \times [0.2, 0.8]$. At the outlet Γ_{OUT}^1 we impose homogeneous Neumann BCs.

As discussed in Subsection 2.2, we imposed non-homogeneous Dirichlet BCs weakly, using Lagrange multipliers. Their space is discretized by means of orthonormal basis functions, built from Chebyshev polynomials. We considered polynomials up to the degree $n_{in} = 5$ to impose inlet BCs, in order to get a good approximation of parabolic velocity profiles. Conversely, we chose $n_{out} = 0$ to impose the outlet BC in the Bifurcation test case, as we are only interested in enforcing the flow rate. The total number of DOFs associated to the Lagrange multipliers is $N_\lambda = 66$ for the Symmetric Bifurcation test case and $N_\lambda = 126$ for the Femoropopliteal Bypass one. Lastly, we remark that in this work we use the *cgs* (centimeter-gram-second) unit system; therefore, the velocity is expressed in (*cm/s*) and the pressure in (*dyn/cm²*), where *dyn* := $g \cdot cm \cdot s^{-2}$. Concerning the computational environment, all simulations were run on the *Scientific IT and Application Support (SCITAS)* clusters¹ at EPFL.

In both test cases, we generated $N_\mu = 50$ training snapshots by solving the FOM problem (see Subsection 2.2) for 50 different parameter values, sampled uniformly at random from \mathcal{D} . We denote with $\mathcal{D}^{train} \subset \mathcal{D}$ the set of training parameters. To compute the FOM solutions, we employed the same computational framework as in [18], which is based on *LifeV*, a C++ FE library with support to high-performance computing [44]. We employed P2-P1 Taylor-Hood Lagrangian finite elements for the discretization of the velocity and pressure subspaces, respectively; we adopted BDF2 as time integrator. The average computational wall time for a single FOM simulation is 1936 s for the Symmetric Bifurcation test case and 6567 s for the Femoropopliteal Bypass one. Table 1 reports the main features of the computational meshes. Concerning the temporal supremizers enrichment, we set $\epsilon_t = 0.5$, unless otherwise specified.

For each test case, we performed $N_\mu^* = 10$ additional FOM simulations in order to evaluate the performances of the proposed ROMs. We define as $\mathcal{D}^{test} := \{\mu_i^*\}_{i=1}^{N_\mu^*}$ the set of test parameters, sampled uniformly at random from \mathcal{D} . Figure 1 shows the velocity magnitude at time $t = 0.13$ s for one test snapshot for each test case. The performances of the proposed ROMs are assessed both in terms of accuracy and of computational efficiency. The former is evaluated considering the average (over the test snapshots) relative errors on velocity and pressure, measured in the norms induced by the symmetric and positive definite matrices \mathbf{X}_u^{st} and \mathbf{X}_p^{st} (see Eq.(3.20), respectively). Therefore, we define:

$$E_u = \frac{1}{N_\mu^*} \sum_{i=1}^{N_\mu^*} \frac{\|\Pi^u \hat{\mathbf{u}}(\mu_i^*) - \mathbf{u}_h^{st}(\mu_i^*)\|_{\mathbf{X}_u^{st}}}{\|\mathbf{u}_h^{st}(\mu_i^*)\|_{\mathbf{X}_u^{st}}} \quad E_p = \frac{1}{N_\mu^*} \sum_{i=1}^{N_\mu^*} \frac{\|\Pi^p \hat{\mathbf{p}}(\mu_i^*) - \mathbf{p}_h^{st}(\mu_i^*)\|_{\mathbf{X}_p^{st}}}{\|\mathbf{p}_h^{st}(\mu_i^*)\|_{\mathbf{X}_p^{st}}} \quad (4.4)$$

being $\hat{\mathbf{w}}(\mu_i^*) = [\hat{\mathbf{u}}(\mu_i^*), \hat{\mathbf{p}}(\mu_i^*), \hat{\lambda}(\mu_i^*)] \in \mathbb{R}^{n^{st}}$ the space-time reduced solution obtained with the considered ROM for the parameter value $\mu_i^* \in \mathcal{D}^{test}$ and $\mathbf{w}_h^{st}(\mu_i^*) = [\mathbf{u}_h^{st}(\mu_i^*), \mathbf{p}_h^{st}(\mu_i^*), \lambda_h^{st}(\mu_i^*)] \in \mathbb{R}^{N^{st}}$ the corresponding FOM

¹<https://www.epfl.ch/research/facilities/scitas/hardware/>

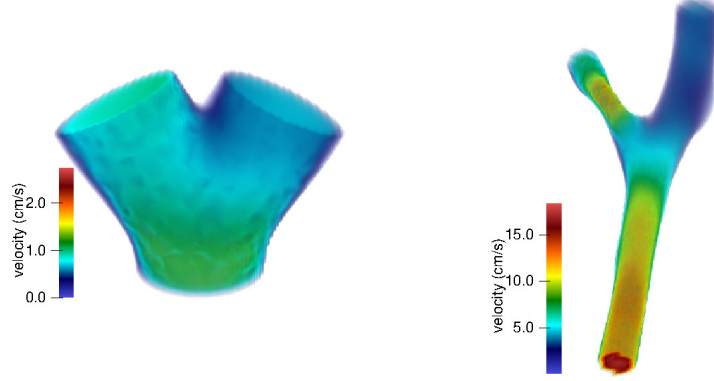


Figure 1. Velocity magnitude of the FOM solution at $t = 0.13$ s for two different test snapshots. In particular: (left) FOM velocity magnitude in the symmetric bifurcation for $\mu^* = [7.18, 0.30, 0.42]$; (right) FOM velocity magnitude in the femoropopliteal bypass for $\mu^* = [5.67, 0.29, 0.24]$.

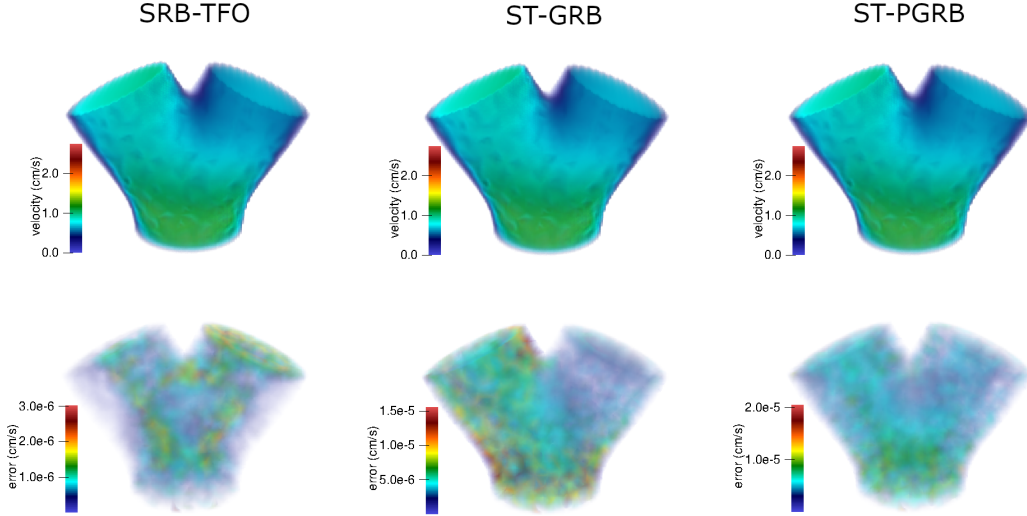


Figure 2. Magnitudes of the velocity fields and corresponding absolute pointwise errors with respect to the FOM solution, achieved in the Symmetric Bifurcation test case with the three considered ROMs for $\epsilon_{POD} = 10^{-5}$, with $\mu^* = [7.18, 0.30, 0.42]$ and at $t = 0.13$ s. In particular: (top) plot of the magnitudes of the velocity fields; (bottom) corresponding absolute pointwise error with respect to the FOM solution.

solution. Notice that Eq.(4.4) applies also to the SRB-TFO method, where no dimensionality reduction in time takes place, by setting the temporal reduced bases as equal to the canonical one. Concerning computational efficiency, we consider two different indicators, namely (1) the *speedup* (SU), defined as the ratio between the average wall time of FOM and of ROM simulations; (2) the *reduction factor* (RF), computed as the ratio between the FOM DOFs (i.e. N^{st}) and the ROM DOFs (i.e. n^{st}).

4.2 Symmetric Bifurcation

Tables 2, 3, 4 report the results got with the three considered ROMs for the Symmetric Bifurcation test case. For each method and for each POD tolerance, we indicate the dimension (in space and in time) of the reduced basis, the *reduction factor*, the *speedup* and the average test relative errors on velocity and pressure (see Eq.(4.4)), normalized with respect to ϵ_{POD} . Figure 2 reports the magnitudes of the velocity fields obtained for $\mu^* = [7.18, 0.30, 0.42]$ (as in Figure 1 – left) with the three considered ROMs at $t = 0.13$ s for $\epsilon_{POD} = 10^{-5}$ (top row) and the corresponding absolute pointwise errors with respect to the FOM solution (bottom row).

The impact of dimensionality reduction in time is evident. Indeed, if we compare the *RF* and the *SU* got with the “standard” SRB-TFO method with the ones achieved with the ST-GRB and ST-PGRB methods, we notice dramatic efficiency gains. For instance, focusing on *SU* and considering $\epsilon_{POD} = 10^{-4}$, the ST-GRB and ST-PGRB methods are roughly 130 and 650 times faster than the SRB-TFO one, respectively. Moreover, the ST-PGRB method is more

ϵ_{POD}	ROM size			Efficiency		Error	
	(n_u^s, n_u^t)	(n_p^s, n_p^t)	$(\{N_{\lambda_k}\}, \{n_{\lambda_k}^t\})$	RF	SU	E_u/ϵ_{POD}	E_p/ϵ_{POD}
10^{-4}	(89,120)	(7,120)	($\{63,3\}, \{120,120\}$)	181	36	1.14	1.09
10^{-5}	(98,120)	(11,120)	($\{63,3\}, \{120,120\}$)	167	29	1.03	0.73
10^{-6}	(108,120)	(16,120)	($\{63,3\}, \{120,120\}$)	154	22	1.10	0.76

Table 2. Summary of the results obtained with the SRB-TFO method on the Symmetric Bifurcation test case, for different POD tolerances ϵ_{POD} . In particular: (left) number of spatial and temporal reduced basis elements for velocity, pressure and Lagrange multipliers; (center) RF and average SU; (right) average test relative errors on velocity and pressure (see Eq.(4.4)), normalized with respect to ϵ_{POD} .

ϵ_{POD}	ROM size			Efficiency		Error	
	(n_u^s, n_u^t)	(n_p^s, n_p^t)	$(\{N_{\lambda_k}\}, \{n_{\lambda_k}^t\})$	RF	SU	E_u/ϵ_{POD}	E_p/ϵ_{POD}
10^{-4}	(89,21 ^{*1})	(7,19)	($\{63,3\}, \{19,16\}$)	1'082	4'650	5.30	4.39
10^{-5}	(98,23)	(11,23)	($\{63,3\}, \{23,20\}$)	875	2'777	5.27	7.89
10^{-6}	(108,25)	(16,25)	($\{63,3\}, \{25,22\}$)	741	1'787	9.70	13.78

Table 3. Summary of the results obtained with the ST-GRB method on the Symmetric Bifurcation test case, for different POD tolerances ϵ_{POD} . In particular: (left) number of spatial and temporal reduced basis elements for velocity, pressure and Lagrange multipliers; (center) RF and average SU; (right) average test relative errors on velocity and pressure (see Eq.(4.4)), normalized with respect to ϵ_{POD} . The notation $(\cdot)^{*n}$ indicates that n temporal supremizers have been added.

ϵ_{POD}	ROM size			Efficiency		Error	
	(n_u^s, n_u^t)	(n_p^s, n_p^t)	$(\{N_{\lambda_k}\}, \{n_{\lambda_k}^t\})$	RF	SU	E_u/ϵ_{POD}	E_p/ϵ_{POD}
10^{-4}	(16,20)	(7,19)	($\{63,3\}, \{19,16\}$)	2'069	23'615	7.61	13.73
10^{-5}	(21,23)	(11,23)	($\{63,3\}, \{23,20\}$)	1'565	11'391	5.89	8.32
10^{-6}	(26,25)	(16,25)	($\{63,3\}, \{25,22\}$)	1'306	7'448	10.37	14.62

Table 4. Summary of the results obtained with the ST-PGRB method on the Symmetric Bifurcation test case, for different POD tolerances ϵ_{POD} . In particular: (left) number of spatial and temporal reduced basis elements for velocity, pressure and Lagrange multipliers; (center) RF and average SU; (right) average test relative errors on velocity and pressure (see Eq.(4.4)), normalized with respect to ϵ_{POD} .

efficient than the ST-GRB one, thanks to its “automatic” *inf-sup* stability property (see Subsection 3.6.2). Indeed, this prevents from the supremizers enrichment of the velocity reduced bases (in space and in time) and it ultimately leads to solve a smaller linear system. The drawback of such an increased computational efficiency is represented by a loss in accuracy. Indeed, while the average relative test errors for the SRB-TFO method are of the order of the POD tolerance, the ones got with the two ST-RB methods are roughly one order of magnitude larger. However, such a behaviour is expected to change if more time instants are considered, either by refining the temporal discretization or by extending the length of the simulation. Indeed, based on the error analysis performed in [16], the stability constant for the SRB-TFO method grows exponentially with N^t , while the one of the ST-GRB method is only $\propto (N^t)^{3/2}$.

Focusing on the ST-GRB method, we remark that for $\epsilon_{POD} = 10^{-4}$ and $\epsilon_t = 0.5$ the velocity temporal reduced basis has been enriched with one supremizer. In particular, the relative errors on velocity and pressure drop of approximately 8 and 140 times, respectively, with respect to the case where no temporal supremizers enrichment is performed. In order to further validate the proposed stabilization procedure, we performed some additional tests, whose results are reported in Table 5. We set $\epsilon_{POD} = 10^{-5}$ for pressure and Lagrange multipliers and $\epsilon_{POD} = 10^{-4}$ for velocity. In this way, the temporal reduced bases for both pressure and Lagrange multipliers feature a larger dimension than the velocity one. As a consequence, the matrices $\Psi^{u,p}, \{\Psi^{u,\lambda_k}\}_{k=1}^{N_D}$ cannot be full column rank and — according to Corollaries 1 – 2 — the temporal supremizers enrichment procedure is compulsory in order to retain *inf-sup* stability with the ST-GRB method. Indeed, if the velocity temporal reduced basis is not augmented, the linear system stemming from

Method	T-sup		ROM size (n_u^s, n_u^t)	Efficiency SU	Error	
	ϵ_t				E_u/ϵ_{POD}	E_p/ϵ_{POD}
SRB-TFO	//	//	(89,120)	32	0.92	0.96
ST-RB	//	//	(89,20)	3'562	6.63e16	7.55e27
	P	0.5	(89,23 ^{*3})	2'962	1.87	17.4
		0.9	(89,26 ^{*6})	2'498	0.97	2.17
	L	0.5	(89,23 ^{*3})	2'926	1.84	14.6
		0.9	(89,27 ^{*7})	2'303	0.97	2.17
ST-PGRB	//	//	(16,20)	13'874	6.68	168
	P	0.5	(16,23 ^{*3})	13'536	2.21	17.5
		0.9	(16,26 ^{*6})	12'414	1.11	1.64

Table 5. Dimensions of the velocity reduced bases, speedups and errors obtained on the Symmetric Bifurcation test case for different temporal supremizers enrichments, setting ϵ_{POD} (in space and in time) to 10^{-5} for pressure and Lagrange multipliers and to 10^{-4} for velocity. Notation: “//” means that no temporal supremizers have been computed, “P” that temporal supremizers enrichment has been performed with respect to pressure, “L” that temporal supremizers enrichment has been performed with respect to Lagrange Multipliers. The notation $(\cdot)^{*n}$ indicates that n temporal supremizers have been added.

the application of the ST-GRB method is ill-conditioned and consequently the errors (on both velocity and pressure) explode. Conversely, if temporal supremizers are added, the problem is stabilized and the errors are comparable with the prescribed POD tolerances.

Three remarks are worth to follow. Firstly, the choice of ϵ_t does influence the results; indeed, for $\epsilon_t = 0.9$ the number of temporal supremizers is doubled with respect to the case $\epsilon_t = 0.5$ and the relative error on pressure drops of approximately one order of magnitude. Secondly, the order in which the dual fields (i.e. pressure and Lagrange multipliers) are considered in order to compute the temporal supremizers does not significantly affect the results. Lastly, in this case the ST-PGRB method, despite being roughly 5 times faster, exhibits worse performances than the (stabilized) ST-GRB one; in particular, the relative error on pressure is two orders of magnitude larger than the prescribed POD tolerance. Nevertheless, accuracies comparable with the ones of ST-GRB can be retrieved by adding temporal supremizers, without severely impacting the efficiency of the method.

4.3 Femoropopliteal Bypass

We now assess the performances of the two considered ST-RB methods on a Femoropopliteal Bypass geometry [41], segmented from CT scans. Tables 6,7 report the results obtained with the ST-GRB and ST-PGRB methods, respectively. In particular, for each POD tolerance, they report the dimension of the reduced bases, the *reduction factor*, the *speedup* and the average test relative errors on velocity and pressure (see Eq.(4.4)), normalized with respect to ϵ_{POD} . Figure 3 reports the magnitude of the velocity, pressure and wall shear stress (WSS) fields obtained for $\mu^* = [5.67, 0.29, 0.24]$ (as in Figure 1 – right) with the ST-PGRB method at $t = 0.13$ s for $\epsilon_{POD} = 10^{-5}$ (top row) and the corresponding absolute pointwise errors with respect to the FOM solution (bottom row).

The performances of both ST-RB methods are good; indeed, they both attain significant computational gains with respect to the FOM and relative errors are approximately one order of magnitude higher than the prescribed POD tolerance. Actually, compared to the previous test cases, the errors are a bit larger. We believe this is mainly caused by the number of snapshots $N_\mu = 50$ that we considered, which may be too low to suitably approximate the solution manifold. However, physical memory limitations prevented us from investigating this aspect any further. As in the Symmetric Bifurcation test case, the ST-PGRB method exhibits better performances than the ST-GRB one, since it produces similar errors while being roughly 5 times faster. Also, we remark that no temporal supremizers enrichment has been necessary to guarantee the *inf-sup* stability of the ST-GRB method, for any of the considered POD tolerances.

5 Conclusions

In this work, we discussed the application of space–time reduced basis methods for the efficient solution of parametrized unsteady incompressible Stokes equations in fixed 3D geometries. Moreover, we supposed the parametric dependency to exclusively characterize the inhomogeneous Dirichlet BCs, that have been weakly imposed by means of Lagrange multipliers. The problem at hand features then a twofold saddle point structure of type 1, as the dual field is a product

ϵ_{POD}	ROM size			Efficiency		Error	
	(n_u^s, n_u^t)	(n_p^s, n_p^t)	$(\{N_{\lambda_k}\}, \{n_{\lambda_k}^t\})$	RF	SU	E_u/ϵ_{POD}	E_p/ϵ_{POD}
10^{-4}	(146,20)	(5,18)	$(\{63,63\}, \{16,17\})$	2'089	5'033	14.30	10.77
10^{-5}	(154,23)	(8,22)	$(\{63,63\}, \{21,21\})$	1'671	2'792	8.87	16.66
10^{-6}	(163,26)	(12,24)	$(\{63,63\}, \{23,24\})$	1'420	1'798	8.77	25.89

Table 6. Summary of the results obtained with the ST-GRB method on the Femoropopliteal Bypass test case, for different POD tolerances ϵ_{POD} . In particular: (left) number of spatial and temporal reduced basis elements for velocity, pressure and Lagrange multipliers; (center) RF and average SU; (right) average test relative errors on velocity and pressure (see Eq.(4.4)), normalized with respect to ϵ_{POD} .

ϵ_{POD}	ROM size			Efficiency		Error	
	(n_u^s, n_u^t)	(n_p^s, n_p^t)	$(\{N_{\lambda_k}\}, \{n_{\lambda_k}^t\})$	RF	SU	E_u/ϵ_{POD}	E_p/ϵ_{POD}
10^{-4}	(15,20)	(5,18)	$(\{63,63\}, \{16,17\})$	4'306	31'272	10.36	23.55
10^{-5}	(20,23)	(8,22)	$(\{63,63\}, \{21,21\})$	3'239	14'925	6.20	17.06
10^{-6}	(25,26)	(12,24)	$(\{63,63\}, \{23,24\})$	2'727	9'802	7.24	31.88

Table 7. Summary of the results obtained with the ST-PGRB method on the Femoropopliteal Bypass test case, for different POD tolerances ϵ_{POD} . In particular: (left) number of spatial and temporal reduced basis elements for velocity, pressure and Lagrange multipliers; (center) RF and average SU; (right) average test relative errors on velocity and pressure (see Eq.(4.4)), normalized with respect to ϵ_{POD} .

space. The high-fidelity problem is obtained by means of a FE discretization of the velocity and pressure subspaces employing P2-P1 Taylor-Hood Lagrangian finite elements and by discretizing the space of Lagrange multipliers with orthonormal basis functions constructed from Chebyshev polynomials. We described the procedure to assemble the spatio-temporal reduced bases, based on the POD algorithm, and we detailed the assembling of the reduced linear system to be ultimately solved. Finally, we focused on the well-posedness of the reduced problem, which is well-known to be troublesome in saddle point problems, since it resorts to *inf-sup* stability analysis. To this end, we proposed two different methods. A first one, called ST-GRB, involves a Galerkin projection and it is characterized by the supremizers enrichment of the spatio-temporal velocity reduced basis. The second one, called ST-PGRB, features instead a Petrov-Galerkin projection, which stems from the minimization of the FOM residual in a suitable norm, so that *inf-sup* stability is “automatically” guaranteed. The performances of the ST-RB methods have been tested on two different test cases, characterized by different geometries (idealized symmetric bifurcation and patient-specific femoropopliteal bypass) and different parametrizations of the Dirichlet datum. Both ST-RB methods showed significant efficiency gains with respect to the baseline space-reduced approach (in terms of both *reduction factor* and *speedup*) and accuracies — with respect to the FOM solution — in accordance with theoretical expectations. In particular, in both test cases the two methods showed comparable accuracies, but ST-PGRB resulted to be roughly 10 times faster than ST-GRB, since the supremizers enrichment procedure could be avoided, without affecting *inf-sup* stability.

Two main limitations can be identified. On the one hand, we focused on a linear problem, neglecting the non-linear convective term that characterizes the Navier-Stokes equations and whose role is of primary importance for the realistic modelling of haemodynamics. On the other hand, we considered fixed geometries, while one major challenge in the numerical approximation of blood flow in patient-specific frameworks is to suitably take into account intra-patient and inter-patient geometrical variability. To this end, we plan to extend the proposed ST-RB approaches to incompressible unsteady Navier-Stokes equations in parametrized 3D geometries, possibly leveraging modular geometrical approximation [18]. RFSI models — as the Coupled Momentum model [45, 42, 43] — and more physiological boundary conditions — as resistance BCs [46, 47] or coronary BCs [48] — could also be valuable tools in order to bridge the gap with clinical applications.

References

- [1] T. Lassila, A. Manzoni, A. Quarteroni, and G. Rozza. Model order reduction in fluid dynamics: challenges and perspectives. *MATHICSE-CMCS Modelling and Scientific Computing*, 2013.

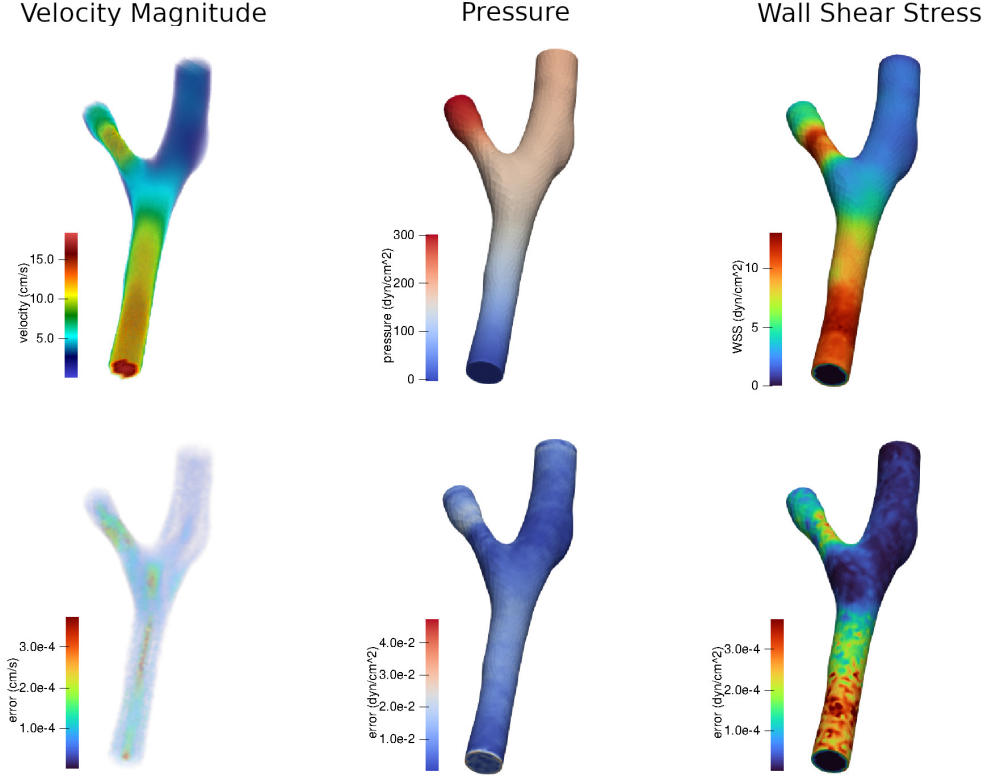


Figure 3. Magnitudes of the velocity (left) pressure (center) and WSS (right) fields, with corresponding absolute pointwise errors with respect to the FOM solution, achieved in the Femoropopliteal Bypass test case with the ST-PGRB method for $\epsilon_{POD} = 10^{-5}$, with $\mu^* = [5.67, 0.29, 0.24]$ and at $t = 0.13$ s. In particular: (top) plot of the magnitudes of the velocity fields, pressure and WSS; (bottom) corresponding absolute pointwise error with respect to the FOM solution.

- [2] Youngsoo Choi and Kevin Carlberg. Space–time least-squares Petrov–Galerkin projection for nonlinear model reduction. *SIAM Journal on Scientific Computing*, 41(1):A26–A58, 2019.
- [3] Petr Krysl, Sanjay Lall, and Jerrold E Marsden. Dimensional model reduction in nonlinear finite element dynamics of solids and structures. *International Journal for numerical methods in engineering*, 51(4):479–504, 2001.
- [4] David J Lucia, Philip S Beran, and Walter A Silva. Reduced–order modeling: new approaches for computational physics. *Progress in aerospace sciences*, 40(1-2):51–117, 2004.
- [5] Zeike A Taylor, Stuart Crozier, and Sébastien Ourselin. Real–time surgical simulation using reduced order finite element analysis. In *International Conference on Medical Image Computing and Computer-Assisted Intervention*, pages 388–395. Springer, 2010.
- [6] Yvon Maday and Gabriel Turinici. A parareal in time procedure for the control of partial differential equations. *Comptes Rendus Mathématique*, 335(4):387–392, 2002.
- [7] Robert D Falgout, Stephanie Friedhoff, Tz V Kolev, Scott P MacLachlan, and Jacob B Schroder. Parallel time integration with multigrid. *SIAM Journal on Scientific Computing*, 36(6):C635–C661, 2014.
- [8] Charbel Farhat and Marion Chandesris. Time–decomposed parallel time–integrators: theory and feasibility studies for fluid, structure, and fluid–structure applications. *International Journal for Numerical Methods in Engineering*, 58(9):1397–1434, 2003.
- [9] Kevin Carlberg, Jaideep Ray, and Bart van Bloemen Waanders. Decreasing the temporal complexity for nonlinear, implicit reduced–order models by forecasting. *Computer Methods in Applied Mechanics and Engineering*, 289: 79–103, 2015.
- [10] Kevin Carlberg, Lukas Brencher, Bernard Haasdonk, and Andrea Barth. Data–driven time parallelism via forecasting. *SIAM Journal on Scientific Computing*, 41(3):B466–B496, 2019.

- [11] Karsten Urban and Anthony T Patera. A new error bound for reduced basis approximation of parabolic partial differential equations. *Comptes Rendus Mathématique*, 350(3-4):203–207, 2012.
- [12] Karsten Urban and Anthony T Patera. An improved error bound for reduced basis approximation of linear parabolic problems. *Mathematics of Computation*, 83(288):1599–1615, 2014.
- [13] Masayuki Yano. A space–time Petrov–Galerkin certified reduced basis method: application to the Boussinesq equations. *SIAM Journal on Scientific Computing*, 36(1):A232–A266, 2014.
- [14] Masayuki Yano, Anthony T Patera, and Karsten Urban. A space–time hp–interpolation–based certified reduced basis method for Burgers’ equation. *Mathematical Models and Methods in Applied Sciences*, 24(09):1903–1935, 2014.
- [15] Y. S. Shimizu and E. J. Parish. Windowed space–time least–squares Petrov–Galerkin model order reduction for nonlinear dynamical systems. *Computer Methods in Applied Mechanics and Engineering*, 386:114050, 2021.
- [16] Y. Choi, P. Brown, W. Arrighi, R. Anderson, and K. Huynh. Space–time reduced order model for large-scale linear dynamical systems with application to Boltzmann transport problems. *Journal of Computational Physics*, 424, 2021.
- [17] Y. Kim, K. Wang, and Y. Choi. Efficient space–time reduced order model for linear dynamical systems in Python using less than 120 lines of code. *Mathematics* 2021, 9(14), 2021.
- [18] Luca Pegolotti, Martin R Pfaller, Alison L Marsden, and Simone Deparis. Model order reduction of flow based on a modular geometrical approximation of blood vessels. *Computer methods in applied mechanics and engineering*, 380:113762, 2021.
- [19] Gabriel N Gatica and Francisco-Javier Sayas. Characterizing the inf–sup condition on product spaces. *Numerische Mathematik*, 109(2):209–231, 2008.
- [20] Jason S Howell and Noel J Walkington. Inf–sup conditions for twofold saddle point problems. *Numerische Mathematik*, 118(4):663–693, 2011.
- [21] Andrea Manzoni. Reduced models for optimal control, shape optimization and inverse problems in haemodynamics. Technical report, EPFL, 2012.
- [22] Alfio Quarteroni, Massimiliano Tuveri, and Alessandro Veneziani. Computational vascular fluid dynamics: problems, models and methods. *Computing and Visualization in Science*, 2(4):163–197, 2000.
- [23] Daniele Boffi, Franco Brezzi, Michel Fortin, et al. *Mixed finite element methods and applications*, volume 44. Springer, 2013.
- [24] Franco Brezzi. On the existence, uniqueness and approximation of saddle–point problems arising from Lagrangian multipliers. *Publications mathématiques et informatique de Rennes*, (S4):1–26, 1974.
- [25] Alfio Quarteroni and Alberto Valli. *Numerical approximation of partial differential equations*, volume 23. Springer Science & Business Media, 2008.
- [26] P Hood and C Taylor. Navier-Stokes equations using mixed interpolation. *Finite element methods in flow problems*, pages 121–132, 1974.
- [27] Alfio Quarteroni, Andrea Manzoni, and Federico Negri. *Reduced basis methods for partial differential equations: an introduction*, volume 92. Springer, 2015.
- [28] Gene H Golub and Charles F Van Loan. *Matrix computations*. JHU press, 2013.
- [29] Nathan Halko, Per-Gunnar Martinsson, and Joel A Tropp. Finding structure with randomness: probabilistic algorithms for constructing approximate matrix decompositions. *SIAM review*, 53(2):217–288, 2011.
- [30] Francesco Ballarin, Andrea Manzoni, Alfio Quarteroni, and Gianluigi Rozza. Supremizer stabilization of POD–Galerkin approximation of parametrized steady incompressible Navier–Stokes equations. *International Journal for Numerical Methods in Engineering*, 102(5):1136–1161, 2015.
- [31] Saifon Chaturantabut and Danny C Sorensen. Nonlinear model reduction via discrete empirical interpolation. *SIAM Journal on Scientific Computing*, 32(5):2737–2764, 2010.
- [32] Simone Deparis. Reduced basis error bound computation of parameter-dependent Navier–Stokes equations by the natural norm approach. *SIAM journal on numerical analysis*, 46(4):2039–2067, 2008.

- [33] Simone Deparis and Gianluigi Rozza. Reduced basis method for multi-parameter-dependent steady Navier–Stokes equations: applications to natural convection in a cavity. *Journal of Computational Physics*, 228(12):4359–4378, 2009.
- [34] Federico Negri, Andrea Manzoni, and Gianluigi Rozza. Reduced basis approximation of parametrized optimal flow control problems for the Stokes equations. *Computers & Mathematics with Applications*, 69(4):319–336, 2015.
- [35] Gianluigi Rozza, DB Huynh, and Andrea Manzoni. Reduced basis approximation and a posteriori error estimation for Stokes flows in parametrized geometries: roles of the inf–sup stability constants. *Numerische Mathematik*, 125(1):115–152, 2013.
- [36] Gianluigi Rozza. On optimization, control and shape design of an arterial bypass. *International Journal for Numerical Methods in Fluids*, 47(10–11):1411–1419, 2005.
- [37] Niccolò Dal Santo and Andrea Manzoni. Hyper-reduced order models for parametrized unsteady Navier–Stokes equations on domains with variable shape. *Advances in Computational Mathematics*, 45(5):2463–2501, 2019.
- [38] Niccolò Dal Santo, Simone Deparis, Andrea Manzoni, and Alfio Quarteroni. An algebraic least squares reduced basis method for the solution of nonaffinely parametrized Stokes equations. *Computer Methods in Applied Mechanics and Engineering*, 344:186–208, 2019.
- [39] Kevin Carlberg, Matthew Barone, and Harbir Antil. Galerkin v. least-squares Petrov–Galerkin projection in nonlinear model reduction. *Journal of Computational Physics*, 330:693–734, 2017.
- [40] Assyr Abdulle and Ondrej Budáč. A Petrov–Galerkin reduced basis approximation of the Stokes equation in parametrized geometries. *Comptes Rendus Mathématique*, 353(7):641–645, 2015.
- [41] Emilie Marchandise, Paolo Crosetto, Christophe Geuzaine, Jean-François Remacle, and Emilie Sauvage. Quality open source mesh generation for cardiovascular flow simulations. In *Modeling of Physiological Flows*, pages 395–414. Springer, 2012.
- [42] Claudia Maria Colciago, Simone Deparis, and Alfio Quarteroni. Comparisons between reduced order models and full 3D models for fluid–structure interaction problems in haemodynamics. *Journal of Computational and Applied Mathematics*, 265:120–138, 2014.
- [43] Claudia M Colciago and Simone Deparis. Reduced numerical approximation of reduced fluid–structure interaction problems with applications in hemodynamics. *Frontiers in Applied Mathematics and Statistics*, 4:18, 2018.
- [44] Luca Bertagna, Simone Deparis, Luca Formaggia, Davide Forti, and Alessandro Veneziani. The LifeV library: engineering mathematics beyond the proof of concept. *arXiv preprint arXiv:1710.06596*, 2017.
- [45] C Alberto Figueroa, Irene E Vignon-Clementel, Kenneth E Jansen, Thomas JR Hughes, and Charles A Taylor. A coupled momentum method for modeling blood flow in three-dimensional deformable arteries. *Computer methods in applied mechanics and engineering*, 195(41–43):5685–5706, 2006.
- [46] Irene E Vignon-Clementel, C Alberto Figueroa, Kenneth E Jansen, and Charles A Taylor. Outflow boundary conditions for three-dimensional finite element modeling of blood flow and pressure in arteries. *Computer methods in applied mechanics and engineering*, 195(29–32):3776–3796, 2006.
- [47] Irene E Vignon-Clementel, CA Figueroa, KE Jansen, and CA Taylor. Outflow boundary conditions for 3D simulations of non-periodic blood flow and pressure fields in deformable arteries. *Computer methods in biomechanics and biomedical engineering*, 13(5):625–640, 2010.
- [48] Hyun Jin Kim, IE Vignon-Clementel, JS Coogan, CA Figueroa, KE Jansen, and CA Taylor. Patient-specific modeling of blood flow and pressure in human coronary arteries. *Annals of biomedical engineering*, 38(10):3195–3209, 2010.

A ST-PGRB method: the assembling phase

In this appendix, we show how the left-hand side matrix $\hat{\mathbf{A}}^{pg}$ and the right-hand side vector $\hat{\mathbf{F}}^{pg}$ of the linear system arising from the application of the ST-PGRB method (see Eq.(3.41)) can be efficiently computed, leveraging the block structure of the problem at hand. We define the diagonal preconditioners of the spatio-temporal norm matrices for velocity, pressure and Lagrange multipliers as $\mathbf{P}_{\mathbf{X}_u}^{st}$, $\mathbf{P}_{\mathbf{X}_p}^{st}$, $\mathbf{P}_{\mathbf{X}_\lambda}^{st}$, respectively. In addition, we define the diagonal preconditioners of the spatial norm matrices for velocity, pressure and Lagrange multipliers as $\mathbf{P}_{\mathbf{X}_u}$, $\mathbf{P}_{\mathbf{X}_p}$, $\mathbf{P}_{\mathbf{X}_\lambda}$, respectively. We recall that $\mathbf{X}_\lambda = \mathbf{P}_{\mathbf{X}_\lambda} = \mathbf{I}_{N_\lambda}$. Firstly, let us consider the left-hand side matrix $\hat{\mathbf{A}}^{pg}$. Exploiting the block structure of the FOM left-hand side matrix \mathbf{A}^{st} (see Eq.(2.11)), we have

$$\hat{\mathbf{A}}^{pg} = \begin{bmatrix} \hat{\mathbf{A}}_{1,1}^{pg} + \hat{\mathbf{A}}_{4,4}^{pg} + \hat{\mathbf{A}}_{7,7}^{pg} & \hat{\mathbf{A}}_{1,2}^{pg} & \hat{\mathbf{A}}_{1,3}^{pg} \\ \left(\hat{\mathbf{A}}_{1,2}^{pg}\right)^T & \hat{\mathbf{A}}_{2,2}^{pg} & \hat{\mathbf{A}}_{2,3}^{pg} \\ \left(\hat{\mathbf{A}}_{1,3}^{pg}\right)^T & \left(\hat{\mathbf{A}}_{2,3}^{pg}\right)^T & \hat{\mathbf{A}}_{3,3}^{pg} \end{bmatrix} \quad (\text{A.1})$$

The different blocks in Eq.(A.1) have the following expressions

$$\begin{aligned} \hat{\mathbf{A}}_{1,1}^{pg} &= (\mathbf{A}_1^{st} \boldsymbol{\Pi}^u)^T (\mathbf{P}_{\mathbf{X}_u}^{st})^{-1} (\mathbf{A}_1^{st} \boldsymbol{\Pi}^u) & \hat{\mathbf{A}}_{4,4}^{pg} &= (\mathbf{A}_4^{st} \boldsymbol{\Pi}^u)^T (\mathbf{P}_{\mathbf{X}_p}^{st})^{-1} (\mathbf{A}_4^{st} \boldsymbol{\Pi}^u) \\ \hat{\mathbf{A}}_{7,7}^{pg} &= (\mathbf{A}_7^{st} \boldsymbol{\Pi}^u)^T (\mathbf{P}_{\mathbf{X}_\lambda}^{st})^{-1} (\mathbf{A}_7^{st} \boldsymbol{\Pi}^u) & \hat{\mathbf{A}}_{1,2}^{pg} &= (\mathbf{A}_1^{st} \boldsymbol{\Pi}^u)^T (\mathbf{P}_{\mathbf{X}_u}^{st})^{-1} (\mathbf{A}_2^{st} \boldsymbol{\Pi}^p) \\ \hat{\mathbf{A}}_{1,3}^{pg} &= (\mathbf{A}_1^{st} \boldsymbol{\Pi}^u)^T (\mathbf{P}_{\mathbf{X}_u}^{st})^{-1} (\mathbf{A}_3^{st} \boldsymbol{\Pi}^\lambda) & \hat{\mathbf{A}}_{2,2}^{pg} &= (\mathbf{A}_2^{st} \boldsymbol{\Pi}^p)^T (\mathbf{P}_{\mathbf{X}_u}^{st})^{-1} (\mathbf{A}_2^{st} \boldsymbol{\Pi}^p) \\ \hat{\mathbf{A}}_{3,3}^{pg} &= (\mathbf{A}_3^{st} \boldsymbol{\Pi}^\lambda)^T (\mathbf{P}_{\mathbf{X}_u}^{st})^{-1} (\mathbf{A}_3^{st} \boldsymbol{\Pi}^\lambda) & \hat{\mathbf{A}}_{2,3}^{pg} &= (\mathbf{A}_2^{st} \boldsymbol{\Pi}^p)^T (\mathbf{P}_{\mathbf{X}_u}^{st})^{-1} (\mathbf{A}_3^{st} \boldsymbol{\Pi}^\lambda) \end{aligned} \quad (\text{A.2})$$

Let us define the following matrices:

$$\begin{aligned} \bar{\mathbf{A}} &= \mathbf{A} \boldsymbol{\Phi}^u \in \mathbb{R}^{N_u^s \times n_u^s} & \bar{\mathbf{B}}^T &= \mathbf{B}^T \boldsymbol{\Phi}^p \in \mathbb{R}^{N_u^s \times n_p^s} & \bar{\mathbf{B}} &= \mathbf{B} \boldsymbol{\Phi}^u \in \mathbb{R}^{N_u^s \times n_p^s} \\ \bar{\mathbf{M}} &= \mathbf{M} \boldsymbol{\Phi}^u \in \mathbb{R}^{N_u^s \times n_u^s} & \bar{\mathbf{C}}^T &= \mathbf{C}^T \in \mathbb{R}^{N_u^s \times N_\lambda} & \bar{\mathbf{C}} &= \mathbf{C} \boldsymbol{\Phi}^u \in \mathbb{R}^{N_\lambda \times n_u^s} \end{aligned} \quad (\text{A.3})$$

Defining additionally $\overline{\mathbf{M}\mathbf{A}} = \bar{\mathbf{M}} + \frac{2}{3}\delta\bar{\mathbf{A}}$, the blocks in Eq.(A.2) can be assembled as follows:

$$\begin{aligned} \left(\hat{\mathbf{A}}_{1,1}^{pg}\right)_{ij} &= (\mathbf{A}_1^{st} \boldsymbol{\Pi}^u)^T (\mathbf{P}_{\mathbf{X}_u}^{st})^{-1} (\mathbf{A}_1^{st} \boldsymbol{\Pi}^u)_{ij} = (\mathbf{A}_1^{st} \boldsymbol{\Pi}^u)_{i,:}^T (\mathbf{P}_{\mathbf{X}_u}^{st})^{-1} (\mathbf{A}_1^{st} \boldsymbol{\Pi}^u)_{:,j} = \\ &= \left(\bar{\mathbf{M}\mathbf{A}}_{i_s}^T (\mathbf{P}_{\mathbf{X}_u})^{-1} \bar{\mathbf{M}\mathbf{A}}_{j_s}\right) \delta_{i_t, j_t} \\ &+ \left(\bar{\mathbf{M}}_{i_s}^T (\mathbf{P}_{\mathbf{X}_u})^{-1} \bar{\mathbf{M}}_{j_s}\right) \left(\frac{16}{9} (\psi_{i_t}^u)_{:N^t-1} (\psi_{j_t}^u)_{:N^t-1} + \frac{1}{9} (\psi_{i_t}^u)_{:N^t-2} (\psi_{j_t}^u)_{:N^t-2} \right. \\ &\quad \left. - \frac{4}{9} (\psi_{i_t}^u)_{2:N^t-1} (\psi_{j_t}^u)_{:N^t-2} - \frac{4}{9} (\psi_{i_t}^u)_{:N^t-2} (\psi_{j_t}^u)_{2:N^t-1} \right) \end{aligned} \quad (\text{A.4})$$

$$\begin{aligned} \left(\hat{\mathbf{A}}_{4,4}^{pg}\right)_{ij} &= (\mathbf{A}_4^{st} \boldsymbol{\Pi}^u)^T (\mathbf{P}_{\mathbf{X}_p}^{st})^{-1} (\mathbf{A}_4^{st} \boldsymbol{\Pi}^u)_{ij} = (\mathbf{A}_4^{st} \boldsymbol{\Pi}^u)_{i,:}^T (\mathbf{P}_{\mathbf{X}_p}^{st})^{-1} (\mathbf{A}_4^{st} \boldsymbol{\Pi}^u)_{:,j} = \\ &= \left(\bar{\mathbf{B}}_{i_s}^T (\mathbf{P}_{\mathbf{X}_p})^{-1} \bar{\mathbf{B}}_{j_s}\right) \delta_{i_t, j_t} \end{aligned} \quad (\text{A.5})$$

$$\begin{aligned} \left(\hat{\mathbf{A}}_{7,7}^{pg}\right)_{ij} &= (\mathbf{A}_7^{st} \boldsymbol{\Pi}^u)^T (\mathbf{P}_{\mathbf{X}_\lambda}^{st})^{-1} (\mathbf{A}_7^{st} \boldsymbol{\Pi}^u)_{ij} = (\mathbf{A}_7^{st} \boldsymbol{\Pi}^u)_{i,:}^T (\mathbf{P}_{\mathbf{X}_\lambda}^{st})^{-1} (\mathbf{A}_7^{st} \boldsymbol{\Pi}^u)_{:,j} = \\ &= \left(\bar{\mathbf{C}}_{i_s}^T \bar{\mathbf{C}}_{j_s}\right) \delta_{i_t, j_t} \end{aligned} \quad (\text{A.6})$$

$$\begin{aligned} \left(\hat{\mathbf{A}}_{1,2}^{pg}\right)_{ij} &= (\mathbf{A}_1^{st} \boldsymbol{\Pi}^u)^T (\mathbf{P}_{\mathbf{X}_u}^{st})^{-1} (\mathbf{A}_2^{st} \boldsymbol{\Pi}^p)_{ij} = (\mathbf{A}_1^{st} \boldsymbol{\Pi}^u)_{i,:}^T (\mathbf{P}_{\mathbf{X}_u}^{st})^{-1} (\mathbf{A}_2^{st} \boldsymbol{\Pi}^p)_{:,j} = \\ &= \frac{2}{3}\delta \left(\bar{\mathbf{M}\mathbf{A}}_{i_s}^T (\mathbf{P}_{\mathbf{X}_u})^{-1} \bar{\mathbf{B}}_{j_s}^T (\psi_{i_t}^u)^T (\psi_{j_t}^p) - \frac{4}{3} \bar{\mathbf{M}}_{i_s}^T (\mathbf{P}_{\mathbf{X}_u})^{-1} \bar{\mathbf{B}}_{j_s}^T (\psi_{i_t}^u)_{:N^t-1} (\psi_{j_t}^p)_{2,:} \right. \\ &\quad \left. + \frac{1}{3} \bar{\mathbf{M}}_{i_s}^T (\mathbf{P}_{\mathbf{X}_u})^{-1} \bar{\mathbf{B}}_{j_s}^T (\psi_{i_t}^u)_{:N^t-2} (\psi_{j_t}^p)_{3,:} \right) \end{aligned} \quad (\text{A.7})$$

$$\begin{aligned}
(\hat{A}_{1,3}^{pg})_{ij} &= (\mathbf{A}_1^{st} \boldsymbol{\Pi}^u)^T (\mathbf{P}_{\mathbf{X}_u}^{st})^{-1} (\mathbf{A}_3^{st} \boldsymbol{\Pi}^\lambda)_{ij} = (\mathbf{A}_1^{st} \boldsymbol{\Pi}^u)_{i,:}^T (\mathbf{P}_{\mathbf{X}_u}^{st})^{-1} (\mathbf{A}_3^{st} \boldsymbol{\Pi}^\lambda)_{:,j} = \\
&= \frac{2}{3} \delta \left(\overline{\mathbf{M}}_{i_s}^T (\mathbf{P}_{\mathbf{X}_u})^{-1} \overline{\mathbf{C}}_{j_s}^T (\boldsymbol{\psi}_{i_t}^u)^T (\boldsymbol{\psi}_{j_t}^\lambda) - \frac{4}{3} \overline{\mathbf{M}}_{i_s}^T (\mathbf{P}_{\mathbf{X}_u})^{-1} \overline{\mathbf{C}}_{j_s}^T (\boldsymbol{\psi}_{i_t}^u)_{:N^t-1} (\boldsymbol{\psi}_{j_t}^\lambda)_{2:} \right. \\
&\quad \left. + \frac{1}{3} \overline{\mathbf{M}}_{i_s}^T (\mathbf{P}_{\mathbf{X}_u})^{-1} \overline{\mathbf{C}}_{j_s}^T (\boldsymbol{\psi}_{i_t}^u)_{:N^t-2} (\boldsymbol{\psi}_{j_t}^\lambda)_{3:} \right)
\end{aligned} \tag{A.8}$$

$$\begin{aligned}
(\hat{A}_{2,2}^{pg})_{ij} &= (\mathbf{A}_2^{st} \boldsymbol{\Pi}^p)^T (\mathbf{P}_{\mathbf{X}_u}^{st})^{-1} (\mathbf{A}_2^{st} \boldsymbol{\Pi}^p)_{ij} = (\mathbf{A}_2^{st} \boldsymbol{\Pi}^p)_{i,:}^T (\mathbf{P}_{\mathbf{X}_u}^{st})^{-1} (\mathbf{A}_2^{st} \boldsymbol{\Pi}^p)_{:,j} = \\
&= \frac{4}{9} \delta^2 \left((\overline{\mathbf{B}}_{i_s}^T)^T (\mathbf{P}_{\mathbf{X}_p})^{-1} \overline{\mathbf{B}}_{j_s}^T \right) \delta_{i_t, j_t}
\end{aligned} \tag{A.9}$$

$$\begin{aligned}
(\hat{A}_{3,3}^{pg})_{ij} &= (\mathbf{A}_3^{st} \boldsymbol{\Pi}^\lambda)^T (\mathbf{P}_{\mathbf{X}_u}^{st})^{-1} (\mathbf{A}_3^{st} \boldsymbol{\Pi}^\lambda)_{ij} = (\mathbf{A}_3^{st} \boldsymbol{\Pi}^\lambda)_{i,:}^T (\mathbf{P}_{\mathbf{X}_u}^{st})^{-1} (\mathbf{A}_3^{st} \boldsymbol{\Pi}^\lambda)_{:,j} = \\
&= \frac{4}{9} \delta^2 \left((\overline{\mathbf{C}}_{i_s}^T)^T (\mathbf{P}_{\mathbf{X}_p})^{-1} \overline{\mathbf{C}}_{j_s}^T \right) \delta_{i_t, j_t}
\end{aligned} \tag{A.10}$$

$$\begin{aligned}
(\hat{A}_{2,3}^{pg})_{ij} &= (\mathbf{A}_2^{st} \boldsymbol{\Pi}^p)^T (\mathbf{P}_{\mathbf{X}_u}^{st})^{-1} (\mathbf{A}_3^{st} \boldsymbol{\Pi}^\lambda)_{ij} = (\mathbf{A}_2^{st} \boldsymbol{\Pi}^p)_{i,:}^T (\mathbf{P}_{\mathbf{X}_u}^{st})^{-1} (\mathbf{A}_3^{st} \boldsymbol{\Pi}^\lambda)_{:,j} = \\
&= \frac{4}{9} \delta^2 \left((\overline{\mathbf{B}}_{i_s}^T)^T (\mathbf{P}_{\mathbf{X}_p})^{-1} \overline{\mathbf{C}}_{j_s}^T \right) \left((\boldsymbol{\psi}_{i_t}^p)^T \boldsymbol{\psi}_{j_t}^\lambda \right)
\end{aligned} \tag{A.11}$$

Let us now consider the right-hand side vector $\hat{\mathbf{F}}_\mu^{pg}$. Exploiting the block structure of the FOM matrix \mathbf{A}^{st} and of the FOM right-hand side vector \mathbf{F}_μ^{st} (see Eq.(2.11)), we have that

$$\begin{aligned}
\hat{\mathbf{F}}_\mu^{pg} &= (\mathbf{A}^{st} \boldsymbol{\Pi})^T (\mathbf{P}_\mathbf{X}^{st})^{-1} \mathbf{F}_\mu^{st} \\
&= \begin{bmatrix} (\mathbf{A}_1^{st} \boldsymbol{\Pi}^u)^T & (\mathbf{A}_4^{st} \boldsymbol{\Pi}^u)^T & (\mathbf{A}_7^{st} \boldsymbol{\Pi}^u)^T \\ (\mathbf{A}_2^{st} \boldsymbol{\Pi}^p)^T & & \\ (\mathbf{A}_3^{st} \boldsymbol{\Pi}^\lambda)^T & & \end{bmatrix} \left(\begin{bmatrix} \mathbf{P}_{\mathbf{X}_u}^{st} & & \\ & \mathbf{P}_{\mathbf{X}_p}^{st} & \\ & & \mathbf{P}_{\mathbf{X}_\lambda}^{st} \end{bmatrix} \right)^{-1} \begin{bmatrix} \\ \\ \mathbf{F}_3^{st}(\boldsymbol{\mu}) \end{bmatrix} \\
&= \begin{bmatrix} (\mathbf{A}_7^{st} \boldsymbol{\Pi}^u)^T \mathbf{F}_3^{st}(\boldsymbol{\mu}) \\ \\ \end{bmatrix}
\end{aligned} \tag{A.12}$$

as $\mathbf{P}_{\mathbf{X}_\lambda}^{st} = \mathbf{I}_{n_\lambda^{st}}$. From Eq.(2.14), the non-zero block in $\hat{\mathbf{F}}_\mu^{pg}$ — denoted as $\hat{\mathbf{F}}_{7,3}^{pg}(\boldsymbol{\mu})$ — is such that:

$$\hat{\mathbf{F}}_{7,3}^{pg}(\boldsymbol{\mu}) = \left[\left(\hat{\mathbf{F}}_{7,3}^{pg,1}(\boldsymbol{\mu}) \right)^T, \dots, \left(\hat{\mathbf{F}}_{7,3}^{pg,N_D}(\boldsymbol{\mu}) \right)^T \right]^T \in \mathbb{R}^{N_\lambda} \tag{A.13}$$

where, for $k \in \{1, \dots, N_D\}$, $\hat{\mathbf{F}}_{7,3}^{pg,k}(\boldsymbol{\mu}) \in \mathbb{R}^{N_\lambda^k}$ is such that

$$\begin{aligned}
\left(\hat{\mathbf{F}}_{7,3}^{pg,k}(\boldsymbol{\mu}) \right)_i &= \left((\mathbf{A}_7^{st})^k \boldsymbol{\Pi}^u \right)_{i,:}^T \begin{bmatrix} \tilde{\mathbf{g}}_k^s g_k^t(t^1; \boldsymbol{\mu}) \\ \vdots \\ \tilde{\mathbf{g}}_k^s g_k^t(t^{N^t}; \boldsymbol{\mu}) \end{bmatrix} = \begin{bmatrix} \mathbf{C}_{i_s}^k (\boldsymbol{\psi}_{i_t}^u)_1 \\ \vdots \\ \mathbf{C}_{i_s}^k (\boldsymbol{\psi}_{i_t}^u)_{N^t} \end{bmatrix}^T \begin{bmatrix} \tilde{\mathbf{g}}_k^s g_k^t(t^1; \boldsymbol{\mu}) \\ \vdots \\ \tilde{\mathbf{g}}_k^s g_k^t(t^{N^t}; \boldsymbol{\mu}) \end{bmatrix} \\
&= \left((\mathbf{C}_{i_s}^k)^T \tilde{\mathbf{g}}_k^s \right) \left((\boldsymbol{\psi}_{i_t}^u)^T \mathbf{g}_k^t(\boldsymbol{\mu}) \right)
\end{aligned} \tag{A.14}$$

Here $(\mathbf{A}_7^{st})^k$ is the k -th block of \mathbf{A}_7^{st} and $\mathbf{g}_k^t(\boldsymbol{\mu}) \in \mathbb{R}^{N^t}$ is such that $(\mathbf{g}_k^t(\boldsymbol{\mu}))_k = g_k^t(t^j; \boldsymbol{\mu})$, for $j \in \{1, \dots, N^t\}$.